[American Journal of Science, Vol. 301, December, 2001, P. 877–911]

ALKALINE INTRUSIONS IN A NEAR-TRENCH SETTING, FRANCISCAN COMPLEX, CALIFORNIA: CONSTRAINTS FROM GEOCHEMISTRY, PETROLOGY, AND $^{40}AR/^{39}AR$ CHRONOLOGY

DIETER F. MERTZ*, ANDREAS J.WEINRICH*, WARREN D. SHARP**, and PAUL R. RENNE**

ABSTRACT. Small gabbroic bodies intruding metagraywackes and cherts of the Late Mesozoic Franciscan Complex represent small-scale magmatic activity in a trench sedimentary environment or in the accretionary prism itself. At Leech Lake Mountain, located in the eastern Franciscan belt of northern California, interbedded radiolarian cherts and graywackes are locally intruded by Ti-rich alkalic diabase sills. The thicker sills are internally differentiated and display cumulate textures of olivine and augite. Although the diabases and surrounding graywackes were overprinted by blueschist metamorphism as indicated by jadeite-rich clinopyroxene and glaucophane, they show little deformation and good preservation of the mafic igneous minerals. The sills comprize alkali basaltic to hawaiitic compositions, all related by fractionation of olivine (Fo_{84}), augite, and titanomagnetite. The immobile trace elements Th, U, Nb, and the LREE (light Rare Earth Elements) are strongly enriched compared to MORB (Mid-Ocean Ridge Basalt), whereas Y and the HREE (heavy Rare Earth Elements) are depleted. Trace element modeling is consistent with either small degrees of melting of primitive mantle or with 6 to 8 percent of partial melting of depleted MORB mantle, which is enriched by up to 8 percent of a metasomatic melt. About 6 percent of garnet in the mantle source of the diabases can account for the observed HREE fractionation and suggests a depth of melting below the garnet-spinel transition zone at 60 to 80 km. This is in agreement with the reconstructed age and thickness of the oceanic plate the diabases intruded in the Early Cretaceous. Incompatible trace element ratios of the diabases are consistent with a HIMU (high μ)-type mantle source. The Early Cretaceous tectonic setting of the Leech Lake Mountain intrusive rocks along the California continental margin is dominated by rapid, highly oblique subduction. If melt is present beneath the oceanic lithosphere without a thermal anomaly, it may readily percolate upward through conduits opened by transtensional tectonics. Asthenospheric upwelling beneath a fracture zone that is migrating along the continental margin may be a viable alternative. $^{40}Ar/^{39}Ar$ dating of amphibole from a diabase olivine cumulate yields a plateau age of 119.0 ± 0.4 Ma, which is the first reported igneous age for the northern California Franciscan Complex. This age implies rapid subduction and metamorphism a few million years after intrusion of the diabases similar to the southern California Ortigalita Peak intrusion. However, the Leech Lake Mountain intrusive rocks are 25 my older and demonstrate that correlations on the basis of similar lithologies and metamorphic grade are problematic.

INTRODUCTION

Common subduction zone models usually do not consider magmatic activity within near-trench environments or in the forearc or accretionary prism itself. However, recent ODP (Ocean Drilling Project) exploration in the Western Pacific has demonstrated the existence of basaltic sills in forearc sedimentary sequences (Taylor and others, 1995). In this work, near-trench intrusive rocks at Leech Lake Mountain, northern California Coast Ranges (Franciscan Complex) are investigated. The basic questions of this study are:

What does rock chemistry imply regarding fractionation, depth of melting, and source composition?

How do these data fit the inferred structure of the convergent plate margin?

* Institut für Geowissenschaften, Johannes Gutenberg-Universität, 55099 Mainz, Germany
** Berkeley Geochronology Center, 2455 Ridge Road, Berkeley, California 94709

How does the igneous age of the sills relate to the plate tectonic reconstructions of the Cretaceous Californian plate margin?

Why does volcanism occur in a near-trench environment?

PREVIOUS WORK

Chesterman (1963) first mapped the Leech Lake Mountain vicinity. Layman (1977) carried out field and petrological work on Leech Lake Mountain alkalic intrusions. Alkalic sills intruding interbedded graywackes and cherts as well as intrusive and extrusive silicic derivatives are found to be ubiquitous in certain units of the Yolla Bolly terrane of northern California by Jayko, Blake, and Brothers (1986). In her pioneering contribution Echeverria (1980) was the first to emphasize the anomalous nature of these intrusions within plate tectonic theory and the first to suggest possible origins. Both Layman (1977) and Echeverria (1980) have demonstrated the near-trench locus of intrusion. Since such intrusions have not been recognized as a common feature of most subduction complexes, Blake and others (1988) suggested they may be related to a characteristic of the Early Cretaceous Franciscan subduction zone, for example a highly oblique, transtensional setting. This suggestion is consistent with plate tectonic reconstructions of Engebretson, Cox, and Gordon (1985).

GEOLOGICAL SETTING

Western North America had an active continental margin characterized by subduction and terrane accretion since the Mid-Paleozoic (Burchfiel, Cowan, and Davis, 1992). In California the three subparallel geologic provinces (fig. 1) of the Franciscan Complex, the Great Valley sequence, and the Sierra Nevada batholith as part of the Klamath-Sierra-Salinia-arc represent remnants of an ancient arc-trench system that formed during east-dipping subduction from the Late Jurassic through the Tertiary (Cowan and Bruhn, 1992). Subduction ceased in the Miocene after arrival and consumption of the East Pacific Rise and was subsequently replaced by a dextral transform fault plate boundary represented by the San Andreas and related strike-slip fault systems. The Sierra Nevada batholith and related plutonic rocks in the Klamath Mountains are interpreted as the roots of a magmatic arc, the Great Valley Sequence as the sedimentary fill of a forearc basin, and the Franciscan Complex as the on-land record of the ancient accretionary complex that accumulated coeval with the structurally higher Great Valley Sequence from Tithonian to Paleogene (Cowan and Bruhn, 1992). The Franciscan Complex consists of several linear northwest to southeast striking belts of melange and of nappes with a relatively coherent internal structure (Wakabayashi, 1992).

In northern California, the Franciscan Complex is commonly subdivided into three subparallel fault bounded units, the Eastern (Yolla Bolly and Pickett Peak Terranes), the Central, and the Coastal Belt. The Franciscan rocks were regionally metamorphosed at blueschist facies conditions in the structural highest and most deformed units to the east and show a decrease in metamorphic grade through prehnite-pumpellyite facies toward zeolite facies conditions to the west (Blake and others, 1988). The Eastern Franciscan Belt essentially comprizes deformed metasediments and minor metabasalts metamorphosed under blueschist facies conditions. The belt is subdivided into two major units, the Pickett Peak and Yolla Bolly terranes, which are juxtaposed along an east dipping low angle fault (Jayko and Blake, 1989). The structurally higher Pickett Peak terrane, consisting of metagraywackes, quartz-mica schists, and metabasalts, has been interpreted as a fragment of a seamount province or oceanic plateau overlain by continentally derived clastic rocks (Blake and others, 1988). The Yolla Bolly terrane consists of four tectonic units: the Chicago Rock melange, the metagraywacke of Hammerhorn Ridge, the broken formation of Devils Hole Ridge, and the Taliaferro Metamorphic Complex. Both the Hammerhorn Ridge

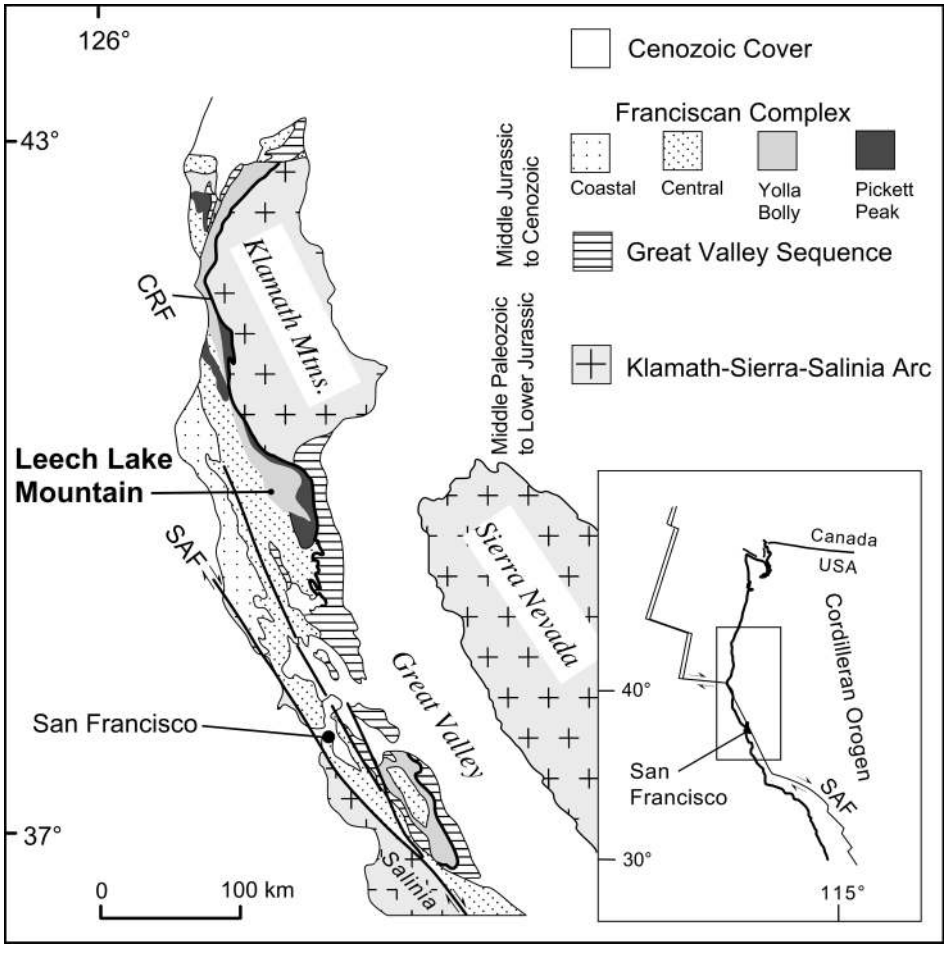

Fig. 1. Geological map of the Franciscan Complex of Northern and Central California (after Moore and Blake 1989). CRF: Coast Range Fault system ; SAF: San Andreas Fault system.

unit and the Taliaferro Complex are intruded locally by Ti-rich alkalic diabase sills and dikes. Additionally, intrusive and extrusive keratophyres have been observed (Jayko et al. 1986). All units of the Yolla Bolly terrane are inferred to be tectonically imbricated, lateral facies equivalents of a continental margin basin that was undergoing minor extension and associated bimodal volcanism due to oblique subduction (Jayko and Blake, 1989).

LEECH LAKE MOUNTAIN REGIONAL GEOLOGY

Leech Lake Mountain is part of the Western Yolla Bolly terrane (fig. 1). The mapped area is presented in figure 2 and contains both the Hammerhorn Ridge unit and the structurally overlying Chicago Rock melange. The Hammerhorn Ridge unit consists predominantly of medium grained graywacke with rare turbiditic structures, ranging from massive to well-bedded. Some prominent layers of red radiolarian chert, partially intruded by the diabases, are interbedded with the graywackes. The chert grades upward into siliceous mudstone, which is in turn overlain by graywacke. Such a sequence typically represents the change from an open ocean to a trench sedimentary

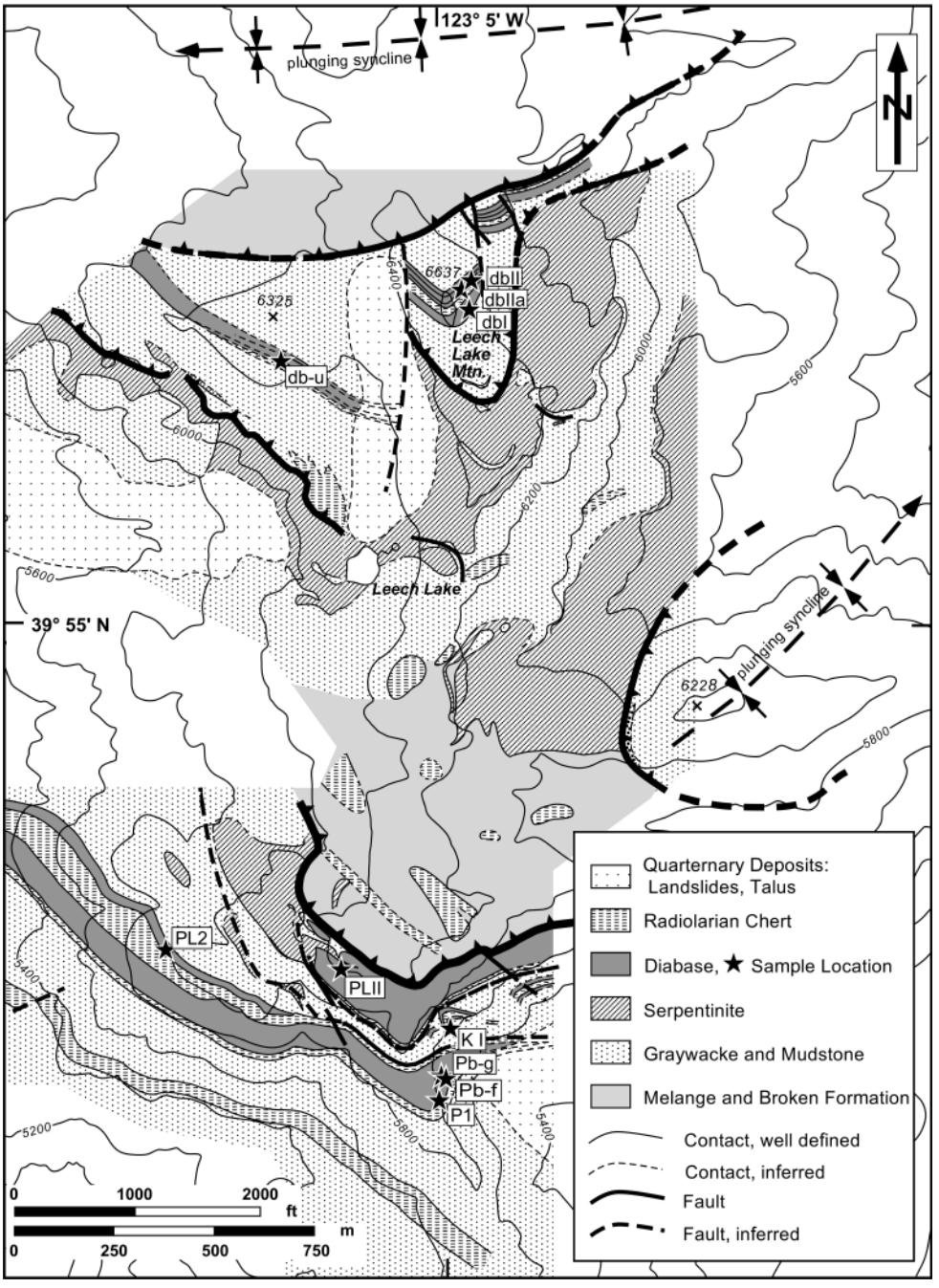

Fig. 2. Geological map of the Leech Lake Mountain area (mapped by A.J.W.). Contour interval m.

environment as the oceanic plate approaches an active continental margin (Isozaki and Blake, 1994). Chert layers often overly graywacke in sharp contact without evidence of shearing or deformation. However, Isozaki and Blake (1994) show for

Yolla Bolly cherts at other localities that apparent coherency of different lithologies at outcrop scale does not necessarily imply a stratigraphic relation, because bedding-parallel faulting can disrupt bedding. Therefore, it is suggested that all contacts between graywacke and overlying chert are tectonic rather than depositional and probably represent duplex structures.

The Chicago Rock melange consists of blocks and slabs of graywacke, greenstone, chert, and carbonate of up to a few meters across in a black to dark gray mudstone matrix that may or may not be sheared. In some places, broken formation with disrupted but still relatively coherent graywacke beds is intercalated with nonbedded, chaotic melange.

Serpentinite bodies, locally with pyroxenitic layers, are emplaced preferentially along major fault contacts. Highly sheared serpentinite occurs where it is squeezed between fault contacts. The serpentinite incorporates numerous rounded blocks or isoclinally folded slabs of graywacke, minor chert, and rare blocks of pegmatitic gabbro. Most contacts between serpentinite and other rocks have a metasomatic zone of more than 0.5 m, which is regarded to be typical for low temperature tectonic contacts (Suppe, 1973).

Diabase sills occur primarily in two areas (fig. 2). On Leech Lake Mountain, four diabase sills were mapped in a fault bounded thrust sheet that is moderately dipping to the northeast. The sills range in thickness up to 30 m and are traceable over a length of about 1.6 km. They are offset by several north-south striking faults. Depositional contacts within the cherts and contacts between mudstone and chert layers served as the preferred sites of intrusion. Sills occurring within graywacke are reported from nearby locations by Isozaki and Blake (1994). Chilled margins are characteristically found at both lower and upper contacts. Beneath the upper chilled margin of the thicker sills, a zone of platy parting perpendicular to the contact extends almost toward the center of the sills. It is caused by oriented growth of long olivine crystals apparently in response to thermal gradients during cooling of the sills.

The second area is about 1.5 km south of Leech Lake Mountain. Two major sequences of sills are separated from each other by tectonized graywackes and serpentinite bodies. The lower sequence extends continously over a length of at least 1.5 km and comprizes a large sill (sill P1) of up to 70 m in thickness and a thinner sill, which is extensively fractured at some localities. Sill P1 is internally differentiated and bears a thick cumulate layer of olivine at its base that is overlain by alternating granular diabase and augite cumulate layers. The upper sequence is truncated on its western side by a steeply dipping fault in contact with serpentinite and is overthrusted by a highly sheared melange unit. It consists of a 20 m thick basal sill and numerous thin sills separated by strongly folded and tectonized cherts and rare graywacke lenses.

ANALYTICAL METHODS

Sample preparation.—Ten samples of the diabases were collected at different locations in order to characterize the overall geochemical variation of these rocks. Depending on grain size, an average of 2 to 3 kg of unaltered rock was collected for each sample. After washing, the rocks were sawed into 5 to 10 cm large chips and crushed in a jaw crusher. The resulting 1 to 2 cm small fragments were handpicked and only pieces free of sawmarks and weathering crust were selected. Subsequent crushing reduced the particle size to less than 5 mm. For XRF and ICP-MS analyses aliquots of 150 to 200 g were then ground to powder in an agate swing mill. For $^{40}Ar/^{39}Ar$ dating kersutitic amphibole and phlogopite from a diabase sill olivine cumulate were prepared. A grain size fraction ranging from 60 to 250 μm was separated by sieving with water. Phlogopite and amphibole were then extracted by magnetic separation and final hand-picking to about 98 percent purity.

X-ray fluorescence.—Major element analyses were performed in the Institut für Geowissenschaften at the University of Mainz using a fully automated Philips PW-1404 wavelength dispersive X-ray fluorescence spectrometer operating with a Rh tube. 0.8 g of sample material was fused with 4.8 g of lithium tetraborate to glass disks. The spectrometer was calibrated with international standards, and mass absorption effects were corrected with alpha coefficients. Accuracy of the major element analyses is within ±2 percent of the working values of Govindaraju (1994) for the international standard BHVO-1. Precision is better than ±1 percent for all elements except Na and Mn where it is within ±2 percent based on 7 replicate analyses of the same glass disk and 6 duplicate analyses using different glass disks.

Electron probe microanalysis.—Mineral compositions were analyzed in the Department of Geology and Geophysics at University of California Berkeley using an eight spectrometer wavelength-dispersive ARL-SEMQ electron microprobe with operating conditions of 15 kV accelerating voltage and 30 nA sample current. Since four spectrometers have fixed monochromator crystals that do not allow off-peak measurement of background intensities, the Mean Atomic Number (MAN) method of Donovan and Tingle (1995) was used for background correction by the integrated software. Based on replicate analyses of international standards precision and accuracy are estimated to be < 2 percent for element oxides with concentrations >5 wt percent and <10 percent for element concentrations from 0.5 to 5 wt percent.

Inductively coupled plasma-mass spectrometry.—Trace element analyses were performed on a VG PlasmaQuad PQ1 ICP-MS in the Geological Department at the University of Kiel following Garbe-Schönberg (1993). Calibration was done with multielement calibration solutions of at least two concentrations covering the expected range within the samples. Mean values ($n = 2$) of the international standard BHVO-1, analyzed together with the samples are compared to recommended values (Govindaraju, 1994, in table 3). Accuracy is better than 10 percent for most of the 36 analyzed elements. Sc, V, Cr, Ni, Zr, Nb, Er, Ta, Pb, and Th are better than 20 percent. For Cs, Tl, and Rb deviation is higher, which can be explained for Cs and Tl by very low concentrations in the standard. Mean values of the Rare Earth Elements and Y in the standard BHVO-1 measured by ICP-MS are systematically lower than the recommended values. Garbe-Schönberg (1993) ascribed this to the fact that the compiled reference values were dominated by XRF data in the past, because a similar bias toward lower values was also found by other analysts using mass spectrometric techniques (Jochum and Seufert, 1990). Precision is specified to be 3 to 5 percent for elements with masses >80 and up to 10 percent for elements with smaller masses (Garbe-Schönberg, 1993).

Gas-source mass spectrometry.—Mineral separates were irradiated wrapped in Cu-foil for 35 hrs at the Oregon State University reactor (CLICIT facility) along with the 28.02 Ma Fish Canyon sanidine standard (Renne and others, 1998). The phlogopite (about 10 mg) and amphibole (about 20 mg) Ar isotope compositions were mass spectrometrically analyzed by incremental heating with a resistance furnace in 19 and 18 steps, respectively, using methods and facilities decribed by Renne (1995). Ages discussed below are given at 1σ and do not include error contributions related to the standard or decay constants but do include error arising from neutron fluence variation. Age calculations are based on IUGS constants (Steiger and Jäger, 1977).

RESULTS

Petrography

In this work the term diabase is used for hypabyssal gabbroic rocks that typically have an ophitic texture and are emplaced as dikes or sills. The mapped diabase sills show no internal deformation in many parts and generally have well preserved igneous

textures. Metamorphic minerals comprize approx 30 to 85 percent of the modal mineral assemblage. Igneous minerals originally were olivine, titanaugite, plagioclase as major components and ilmenite, titanomagnetite, apatite, kaersutitic hornblende, and in one case phlogopite as accessory minerals. A petrographic sample description is given in app. A.

Olivine ranges from very elongated, skeletal to solid equant euhedral crystal shapes and is only preserved in relics in the cumulate. Otherwise it is completely replaced by serpentinite or chlorite. *Titanaugite* ranges from elongated, highly skeletal to euhedral prismatic crystal shapes and is the best preserved igneous phase. It is pinkish due to high Ti content and strongly zoned. Where augite decomposes it is either replaced by patches of highly birefringent aegirine augite or by clustered masses of chlorite, pumpellyite, white mica, and sphene. *Plagioclase* has normally subhedral to euhedral crystal shapes and is typically replaced by albite, jadeite, or white mica. Characteristic polysynthetic twinning is preserved in the larger albitized crystals. Opaque phases are *ilmenite* and *titanomagnetite*. Relic ilmenite is generally well-preserved in the medium to coarse-grained rocks and usually occurs as thinly tabular, often hollow crystals. Titanomagnetite is preserved only in the most coarsely crystalline inner parts of the intrusives and is completely replaced by sphene or leucoxene elsewhere. It can be recognized by its triangular to cubic or cruciform skeletal habit. *Apatite* forms hollow, highly acicular crystals that are typically found in rapidly crystallized rocks. *Kaersutitic amphibole* is dark reddish brown and strongly pleochroic. It occurs as a late magmatic phase mainly in olivine and clinopyroxene cumulates forming patchy replacements within augite as well as euhedral crystals. It is mostly well preserved and frequently rimmed by dark blue ferroglaucophane. *Phlogopite* occurrence is limited to the interstices of the olivine cumulate, indicating that it formed late in the crystallization sequence.

The diabase sills show a systematic variation of textures across their width which might be essentially a result of different cooling rates and degree of supercooling. The thicker sills additionally display internal differentiation by crystal fractionation as indicated by cumulates and by varying modal abundance of ferromagnesian minerals. Typically, grain sizes are smaller than 0.5 mm at the chilled margins and average at 6 to 8 mm in the central portion. The chilled margins are characterized by a microcrystalline groundmass with variable small amounts (<5 percent) of skeletal olivine phenocrysts up to several millimeters in length. Farther inward from the upper chilled margin a porphyritic texture develops with elongated skeletal augite crystals growing in clustered, fan-like aggregates. The fine-grained groundmass consists of small plagioclase laths and probably former augite microcrysts, which are now completely altered. Toward the center of the sills augite crystals become more euhedral prismatic, and plagioclase laths become larger until in the lower part a more gabbroic, subophitic texture is developed with prismatic augite and subhedral plagioclase. In the upper portions of the thicker sill a large zone is developed that macroscopically exhibits a platy parting perpendicular to the sill contacts, caused by a mineral growing in thin plate-like morphologies, stacked to subparallel or slightly divergent aggregates. The mineral is now completely serpentinized and could have been either olivine or a low calcium pyroxene, for example, pigeonite. This texture resembles the plate spinifex texture known from komatiites (Donaldson, 1982; Renner and others, 1994). Additionally, in the center of a 30 m thick sill at the crest of Leech Lake Mountain (fig. 2) up to 50 cm long augite crystals, oriented perpendicular to the margin, are observed. They form a zone several meters in thickness that reaches from the center of the sill upward with decreasing length and diameter of the augite crystals. In the large sill in the southern part of the mapped area (fig. 2) the basal chilled margin is overlain by a medium grained olivine cumulate of equant olivines. Irregular oikocrysts of augite up to 4 mm in diameter are variably replaced by late magmatic brown kaersutite and

enclose the best preserved olivine. Prismatic apatite, phlogopite, titanomagnetite, and ilmenite fill the intercumulus space. The olivine cumulate, approx 15 m thick, grades into an augite cumulate, consisting of euhedral, prismatic augites up to 10 mm in length.

Mineral Chemistry

Representative analyses of measured minerals are listed in table 1. *Olivine* as the first crystallizing phase is abundant in most samples. Cumulate olivines range in composition from forsterite 81.0 to 84.1 percent and are slightly zoned with more magnesian cores. The known olivine compositions were used to calculate a whole-rock Mg-number (Mg# = Mg/(Mg + Fe^{2+}) in equilibrium with the olivine using Roeder and Emslie's (1970) Fe^{2+}-Mg exchange distribution coefficient ($K_D = (Fe^{2+}/Mg)_{olivine}/(Fe^{2+}/Mg)_{melt} = 0.30 \pm 0.03$). Melts that are in equilibrium with the most magnesian cumulus olivine (Fo = 84.1) should have Mg-numbers ranging from 59 to 64 depending on K_D (0.27-0.33). These Mg-numbers are matched by the analyzed samples db II (Mg# = 58; this work) and LL30C (Mg# = 60; Layman, 1977). Therefore, these samples may represent the original composition of the intruding magma of sill P1 before it internally differentiated. This magma, however, could not have been primary, because magmas in equilibrium with typical mantle olivine (Fo = 88-90; Arai, 1987) should have Mg#'s of 67 to 75. Thus, the magma of the sills has most likely undergone olivine fractionation prior to emplacement.

The only magmatic *pyroxene* found is a pinkish, strongly zoned titanaugite. Using the pyroxene quadrilateral (fig. 3) for classification, all measured pyroxenes plot as Ca-rich augites or as diopsides (salites) showing a moderate iron enrichment trend parallel to the diopside hedenbergite join. Such a horizontal fractionation trend is characteristic for clinopyroxenes from alkalic, silica-undersaturated rocks, whereas those from tholeiitic, silica-saturated rocks become increasingly subcalcic with iron enrichment (Robinson, 1980). Concentrations of the non-quadrilateral components Ti (0.86-4.52 wt percent TiO_2) and Al (0.8-10 wt percent Al_2O_3) are high and generally increase toward the rim of crystals, indicating a high proportion of Ti-tschermaks substitution. High Al and Ti contents in clinopyroxenes are ascribed to several factors. Rapid crystal growth is a stimulus for Al substitution whereas the Ti content appears to be more dependent on bulk rock chemistry than on growth rate (Donaldson, 1982). Al substitution in clinopyroxene is also favored where plagioclase crystallization is delayed or prevented, because the Al content of the melt remains high, and the pyroxene does not have to compete for Al (Robinson, 1980). This is consistent with the late occurrence of plagioclase in the crystallization sequence of the Leech Lake Mountain intrusive rocks. Other Al determining factors are silica activity and pressure (Simonetti, Shore, and Bell, 1996). Silica undersaturation favors tetrahedral Si substitution by Al, whereas increasing pressure causes preferred Al substitution on the octahedral site, resulting in an increasing Al^{VI}/Al^{IV} ratio. Al^{VI}/Al^{IV} ratios of 0 to 0.7 in the Leech Lake Mountain clinopyroxenes favor low pressure crystallization. Summarized, clinopyroxene composition is consistent with rapid growth rates, with low silica activity and with a low pressure of crystallization.

Igneous *amphibole* is found in relative abundance in the olivine and clinopyroxene cumulates. Ti content ranges from 0.4 to 0.69 atoms per formula unit (pfu) and, therefore, allows us to classify it as kaersutite (Leake, 1978). Other non-quadrilateral components are Al (1.76-2.22 atoms pfu) and Na (0.78-1.08 atoms pfu). Toward the rims of many kaersutites Ti, Al, Ca decrease whereas Na, Fe, Si increase. This reflects a continous transition from calcic to sodic-calcic barroisitic amphibole and is attributed to deuteric alteration caused by water-rich fluids from the crystallizing magma, although barroisitic amphibole has also been considered a high-pressure meatorphic phase (Ernst, 1979; Evans, 1990).

TABLE 1

Representative igneous mineral microprobe analyses

	Olivine		Oxides			
Sample	P1	P1	db I	P1	P1	P1
SiO_2	39.51	39.72	0.06	0.06	0.12	0.02
TiO_2	0.06	0.01	51.54	51.42	12.03	4.14
Al_2O_3	0.05	0.09	0.11	0.20	5.07	13.12
Cr_2O_3	0.04	0.07	0.02	0.47	11.50	34.44
FeO	15.24	16.56	45.94	38.41	62.53	38.15
MnO	0.19	0.24	1.06	0.43	0.37	0.27
MgO	45.10	43.32	1.10	8.51	5.11	8.54
CaO	0.30	0.28	0.02	0.06	0.00	0.00
NiO	0.27	n.d. *	n.d.	n.d.	n.d.	n.d.
Total	100.26	99.98	99.87	99.56	96.72	98.68
Si	0.99	1.00	0.00	0.00	0.00	0.00
Ti	0.00	0.00	0.97	0.92	0.32	0.10
Al	0.00	0.00	0.00	0.01	0.21	0.51
Cr	0.00	0.00	0.00	0.01	0.32	0.90
Fe^{3+}	0.00	0.00	0.05	0.15	0.82	0.38
Fe^{2+}	0.32	0.35	0.91	0.61	1.04	0.68
Mn	0.00	0.01	0.02	0.01	0.01	0.01
Mg	1.68	1.63	0.04	0.30	0.27	0.42
Cations	3.01	3.00	2.00	2.00	3.00	3.00
Cr# **					0.60	0.64
Mg# ***	0.84	0.82	0.04	0.33	0.21	0.38

	Clinopyroxene				Amphibole		Phlogopite
Sample	db I rim	P1 core	PL 2 rim	PL 2 core	LLM 34A	P1	P1
SiO_2	44.43	50.24	42.76	48.96	40.31	43.39	37.90
TiO_2	3.70	1.86	4.44	1.81	5.10	4.70	5.46
Al_2O_3	9.35	5.05	9.67	4.96	12.36	10.68	14.70
Cr_2O_3	0.31	0.41	0.02	0.37	0.00	0.07	0.04
FeO	8.51	5.37	9.79	6.50	13.49	8.30	8.60
MnO	0.12	0.10	0.16	0.13	0.17	0.10	0.05
MgO	11.99	15.20	10.93	14.65	11.21	15.79	19.08
CaO	21.05	22.21	21.00	21.76	11.07	10.75	0.00
Na_2O	0.55	0.33	0.55	0.34	3.00	3.47	1.44
K_2O	0.00	0.00	0.00	0.00	0.93	0.73	8.40
Total	100.01	100.78	99.33	99.49	97.64	97.91	95.67
Si	1.66	1.83	1.62	1.82	6.03	6.26	2.73
Al^{IV}	0.34	0.17	0.38	0.18	1.97	1.74	1.25
Al^{VI}	0.07	0.05	0.05	0.03	0.21	0.07	0.00
Ti	0.10	0.05	0.13	0.05	0.57	0.51	0.30
Fe^{3+}	0.10	0.03	0.12	0.06	0.00	0.21	n.d.
Fe^{2+}	0.17	0.14	0.19	0.14	1.69	0.79	0.52
Mn	0.00	0.00	0.01	0.00	0.02	0.01	0.00
Mg	0.67	0.83	0.62	0.81	2.50	3.40	2.05
Ca	0.84	0.87	0.85	0.87	1.78	1.66	0.00
Na	0.04	0.02	0.04	0.02	0.88	0.98	0.20
K	0.00	0.00	0.00	0.00	0.18	0.13	0.77
Cations	4.00	4.00	4.00	4.00	15.83	15.77	7.83

Olivine calculated on the basis of 4 oxygens, oxides on the basis of 4 oxygens and 3 cations, clinopyroxene on the basis of 6 oxygens and 4 cations, amphibole on the basis of 23 oxygens and 13 cations excluding Ca, Na, and K, phlogopite on the basis of 11 oxygens. Fe^{3+} was determined by charge balance. Calculations are done using Minpet software version 2.02.

*n.d. = not determined; **Cr# = Cr/(Cr + Al); ***Mg# = Mg/(Mg + Fe^{2+}).

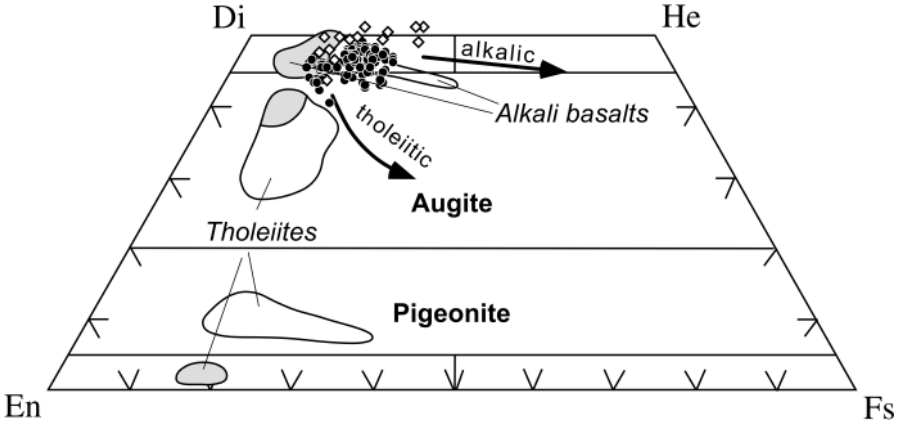

Fig. 3. Clinopyroxene compositions of the Leech Lake Mountain intrusive rocks (closed circles) and from Vesteris seamount (Haase and Devey 1994, open diamonds) as well as from Hawaiian tholeiitic and alkalic basalts for comparison. White fields: groundmass; grayed fields: megacrysts (after Basaltic Volcanism Study Project, 1981, p.184).

Phlogopite occurrence is limited to the interstices of the olivine cumulate, indicating that it formed late in the crystallization sequence after the residual melt was sufficiently enriched in K and H_2O to stabilize it. Its high magnesium-number ($Mg/(Mg+Fe) = 0.8$) is identical to that of the cumulate and confirms a magmatic origin. High Ti contents (3.6-6.0 wt percent) reflect the magma composition.

Ilmenite and *titanomagnetite* are abundant opaque phases in the diabases. Titanomagnetite was analyzed in the olivine containing up to 5.0 percent Al_2O_3, 5.8 percent MgO, and 12 percent Cr_2O_3. Cr spinel was found inside serpentinized cumulus olivine crystals and in some augite crystals. Ilmenite is generally much better preserved than titanomagnetite. The olivine cumulate has ilmenites with the highest MgO (6-9 wt percent) and Fe_2O_3 (5-7 wt percent) content, whereas all other ilmenites have 0-4 wt percent MgO and 1.7-4.3 wt percent Fe_2O_3.

Major Elements

Table 2 presents major element concentrations and CIPW norm calculations of the Leech Lake Mountain diabases. The samples were classified using two diagrams. The total alkali-silica (TAS) diagram of Cox, Bell, and Pankhurst (1979) (fig. 4A) strictly applies only to unaltered rocks, because the discriminating elements are mobile in response to alteration or low grade metamorphism. However, with two exceptions the samples form a tight trend that spans the alkali basalt and hawaiite field ranging in SiO_2 from 46 to 51 percent at alkali contents of 3.7 to 7.2 percent, indicating no significant alteration. The Zr/TiO_2-Nb/Y diagram of Winchester and Floyd (1977) (fig. 4B) has been effectively used in identifying basaltic magma types, because these elements are relatively immobile under low-grade metamorphic conditions. Our samples plot close together in the alkali basalt field.

Most Leech Lake Mountain diabase analyses contain normative nepheline up to a maximum of about 7 percent, confirming the alkaline affinity of the rocks. The most strongly altered sample (PL2) is quartz normative. The olivine cumulate (sample P1) is characterized by high amounts of normative hypersthene that can be explained by an approx 0.8 percent loss of Na_2O and a small gain of SiO_2.

Major element diabase variations are plotted in figure 5 together with fields of selected rock suites from literature for comparison. Generally, the major elements that

TABLE 2

Major element XRF analyses on Leech Lake Mountain diabases

Sample	db I	db II	db IIa	db-u	K I	P1	Pb-f	Pb-g	PL II	PL2
					Original XRF analyses					
SiO_2	46.04	44.87	43.37	47.38	45.49	38.61	46.00	50.19	45.63	46.51
TiO_2	3.54	3.59	3.70	3.19	2.88	1.20	3.76	2.51	3.25	3.59
Al_2O_3	14.84	12.11	12.50	15.57	9.33	4.51	13.88	15.12	12.45	14.21
Fe_2O_3	13.19	13.55	13.26	11.89	11.82	14.55	13.96	11.95	13.57	11.81
MnO	0.16	0.23	0.16	0.24	0.15	0.17	0.28	0.21	0.21	0.14
MgO	4.96	8.06	6.11	3.46	11.08	28.47	5.11	3.37	6.66	3.71
CaO	8.38	9.95	11.57	7.24	13.26	3.58	7.13	6.28	9.64	11.39
Na_2O	4.73	2.72	2.81	5.22	1.61	0.19	3.55	4.92	3.63	2.93
K_2O	1.15	0.84	1.77	0.93	1.34	0.32	2.36	2.11	0.75	0.51
P_2O_5	0.61	0.57	1.03	0.81	0.37	0.19	0.78	0.87	0.56	0.68
LOI	2.61	3.30	3.63	3.39	2.63	8.27	2.82	2.37	3.07	4.71
Total	100.21	99.79	99.91	99.32	99.94	100.03	99.63	99.90	99.42	100.19
					Analyses, normalized on a waterfree basis					
SiO_2	47.28	46.42	45.02	49.07	46.73	42.13	47.36	51.42	47.10	48.83
TiO_2	3.64	3.71	3.84	3.30	2.95	1.30	3.87	2.57	3.35	3.77
Al_2O_3	15.24	12.53	12.98	16.13	9.58	4.92	14.29	15.49	12.85	14.92
Fe_2O_3	2.88	2.14	2.10	2.62	1.85	1.89	3.05	2.93	2.14	1.89
FeO	9.60	10.69	10.50	8.72	9.26	12.59	10.18	8.38	10.68	9.45
MnO	0.16	0.24	0.17	0.25	0.15	0.18	0.29	0.22	0.22	0.15
MgO	5.09	8.34	6.34	3.58	11.38	31.07	5.26	3.46	6.87	3.89
CaO	8.61	10.29	12.01	7.50	13.62	3.90	7.34	6.44	9.95	11.96
Na_2O	4.86	2.81	2.92	5.41	1.65	0.21	3.65	5.04	3.75	3.08
K_2O	1.18	0.87	1.84	0.96	1.38	0.34	2.43	2.16	0.77	0.54
P_2O_5	0.63	0.59	1.07	0.84	0.37	0.20	0.80	0.89	0.58	0.71
Total	99.17	98.64	98.78	98.38	98.93	98.74	98.53	98.99	98.27	99.19
Fe_2O_3/FeO *	0.30	0.20	0.20	0.30	0.20	0.15	0.30	0.35	0.20	0.20
Mg# **	48.6	58.2	51.9	42.3	68.7	81.5	47.9	42.4	53.4	42.3
					CIPW ***					
Q	0	0	0	0	0	0	0	0	0	1.22
Or	7.04	5.22	11.02	5.77	8.25	2.04	14.59	12.91	4.64	3.22
Ab	28.58	24.08	12.97	39.82	9.90	1.80	28.27	41.11	27.21	26.25
An	16.39	19.24	17.05	17.14	14.79	11.61	15.63	13.36	16.21	25.45
Ne	6.96	0	6.51	3.60	2.28	0	1.65	1.04	2.73	0
Di	18.81	23.59	30.21	12.96	41.24	5.42	13.60	11.30	25.03	24.96
Hy	0	1.08	0	0	0	16.69	0	0	0	7.35
Ol	9.65	15.20	9.41	8.60	14.36	56.73	12.53	9.10	13.25	0
Mt	4.21	3.15	3.08	3.86	2.71	2.78	4.50	4.29	3.16	2.76
Il	6.97	7.15	7.39	6.37	5.67	2.50	7.46	4.93	6.48	7.22
Ap	1.39	1.31	2.36	1.86	0.82	0.44	1.77	1.96	1.29	1.56
Total	100.00	100.02	100.00	99.98	100.02	100.01	100.00	100.00	100.00	99.99

LOI = Loss on ignition; *Fe_2O_3/FeO ratios used in CIPW and Mg number calculations from Middlemost (1989); **Mg# = $100 \times Mg/(Mg + Fe^{2+})$; ***CIPW norms calculated using Minpet software version 2.02.

are mobile in response to alteration and low grade metamorphism (SiO_2, CaO, Na_2O, K_2O) display significantly larger scatter than the more immobile elements (MgO, FeO, Al_2O_3, TiO_2, P_2O_5). The MgO content of the Leech Lake Mountain intrusives ranges from 8.6 to 3.5 percent, and is as high as 31.1 percent in the cumulates. Several fractionation trends are recognized. SiO_2, Al_2O_3, Na_2O, K_2O, and P_2O_5 are increasing with decreasing MgO, and CaO is continously decreasing. TiO_2 and FeO first show a slight increase and a sharp drop at 5 percent MgO. An inflection at 5 percent MgO is

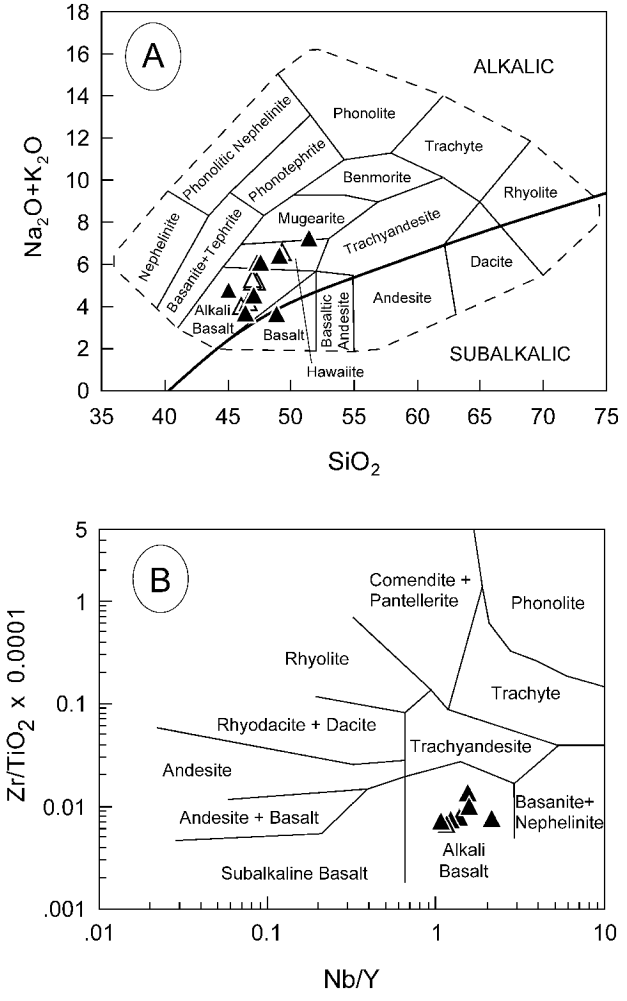

Fig. 4. Rock classification diagrams on the basis of major and trace elements. Filled triangles: samples from this work; open triangles: samples from Layman (1977). (A) Total-Alkali-Silica diagram. Curved solid line (Kuno 1966) subdivides alkaline from subalkaline rocks. Cumulate rocks are not plotted, because they do not reflect liquid compositions (B) Zr/TiO_2 - Nb/Y diagram.

recognized for most other elements as well. Compared to the compiled literature data, compositions of the Leech Lake Mountain intrusives are similar to those of Tahiti, representing typical moderately to highly alkaline oceanic island rocks.

Trace Elements

Diabase trace element concentrations are presented in table 3. Compatible trace elements (Cr, Ni, Sc, Co, Cu, Zn) are high in the primitive rocks and cumulates and are rapidly depleted in the more fractionated samples. The other elements behave incompatibly and their concentrations increase during fractional crystallization.

The elements Rb, Ba, K, Pb, and Sr show a large scatter among different samples in a primitive mantle-normalized multi-element diagram (fig. 6A) indicating that they were mobile. In contrast, all other elements produce subparallel patterns and are

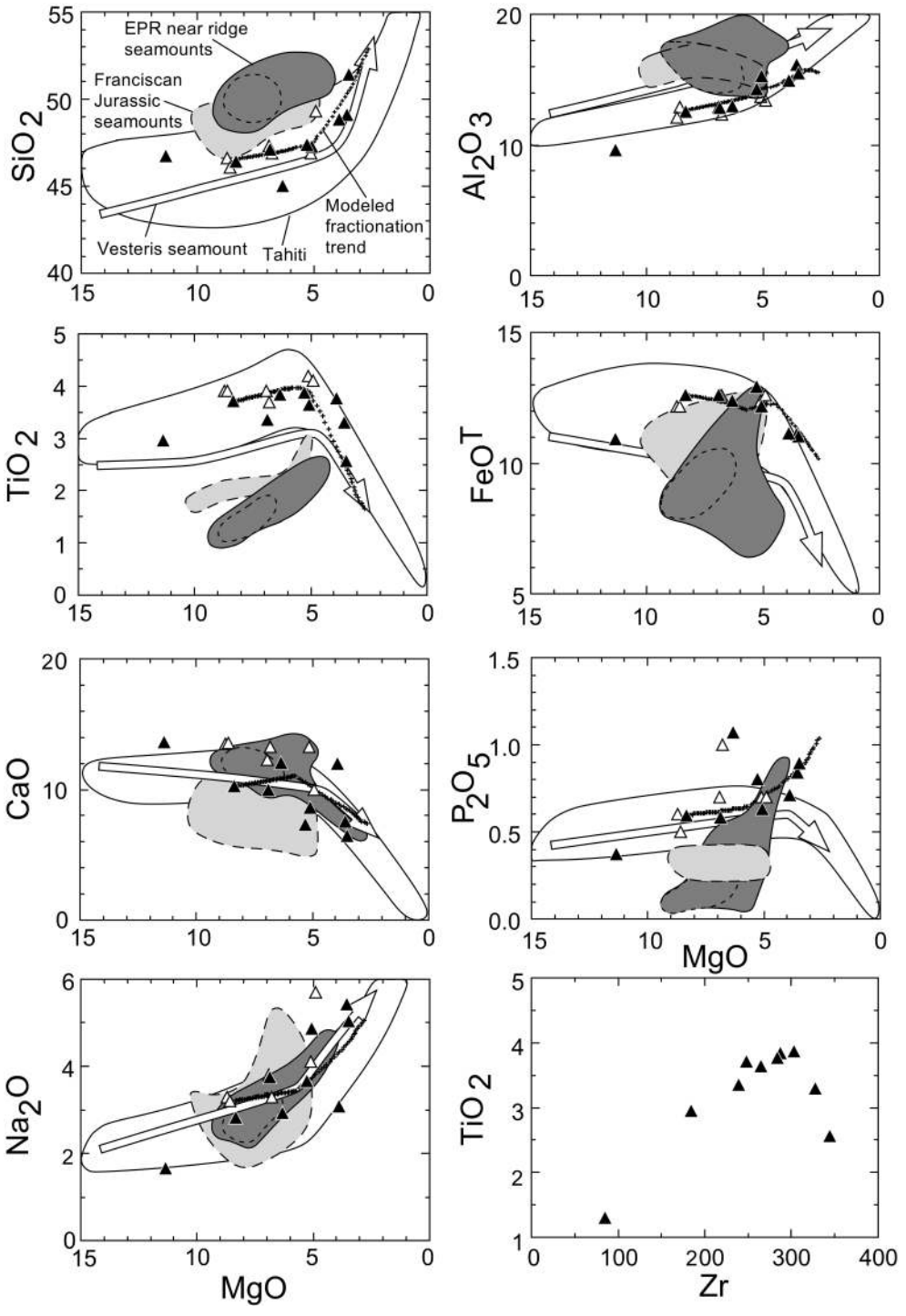

Fig. 5. Major element variation diagrams for the Leech Lake Mountain intrusive rocks and selected oceanic basalts. Filled triangles: Leech Lake Mountain, this work; open triangles: Leech Lake Mountain, Layman (1977). EPR (East Pacific Rise) seamount samples (n = 80) from Batiza and Vanko (1984). Dashed line within the EPR seamount field encloses roughly 75 percent of the data. Franciscan Jurassic seamount samples (n = 16) from McPherson (1983), Shervais and Kimbrough (1987), and Shervais and Hanan (1989). Tahiti samples (n = 105) from Duncan and others (1994). Vesteris seamount samples (n = 17) from Haase and Devey (1994). Unit is wt percent, except for Zr which is ppm. Line of small crosses represents the best-fit fractionation trend modeled using MELTS.

TABLE 3

Trace element concentrations of the Leech Lake Mountain diabases

Sample	P1	db II	Pb-f	Pb-g	PL2	BHVO-1 *			N-type	MORB***
						Measured value	Working value	Deviation**		
Li	15.3	23.8	18.5	15.4	17.8	4.26	4.6	-7.35		n.d.****
Sc	8.7	21.7	7.2	6.1	17.8	26.89	31.8	-15.46		41.37
V	180	273	219	122	284	375	317	18.31		n.d.
Cr	1444	284	0	0	123	239	289	-17.40		n.d.
Co	109.2	42.4	40.1	26.6	36.6	44.77	45	-0.51		47.07
Ni	1530	103	12	4	42	107	121	-11.34		149.5
Cu	22.9	84.8	39.1	22.5	139.2	131	136	-3.4		74.4
Zn	104.82	126.22	132.80	168.95	114.11	115	105	9.13		n.d.
Ga	7.97	20.90	24.91	27.24	24.92	20.28	21	-3.41		n.d.
Zr	73	222	201	293	237	161	179	-10.19		104.24
Hf	2.02	6.29	4.98	7.05	6.23	4.60	4.38	4.98		2.974
Nb	8.74	27.93	27.80	41.98	24.08	16.27	19	-14.35		3.507
Ta	0.59	1.87	1.65	2.47	1.42	1.04	1.23	-15.23		0.192
Rb	4.4	10.3	19.6	18.4	5.2	8.55	11	-22.29		1.262
Sr	83	160	135	194	862	391	403	-3.05		113.2
Cs	1.86	0.94	0.94	1.47	0.40	0.10	0.13	-25.44		0.01408
Ba	50	111	538	428	83	133	139	-4.32		13.87
Tl	0.02	0.17	0.08	0.06	0.02	0.04	0.06	-32.07		n.d.
Pb	0.58	1.71	0.92	2.12	1.66	2.30	2.6	-11.68		0.489
Th	0.59	1.87	1.77	2.94	2.04	1.29	1.08	19.71		0.1871
U	0.27	0.85	0.90	1.38	1.12	0.44	0.42	5.36		0.0711
Y	8.7	24.8	21.6	30.7	26.2	25.68	27.6	-6.97		35.82
La	7.3	22.2	25.4	36.9	26.0	15.31	15.8	-3.09		3.895
Ce	17.1	51.7	60.7	82.7	58.5	36.81	39	-5.61		12.001
Pr	2.40	7.39	8.08	11.37	7.99	5.44	5.7	-4.51		2.074
Nd	10.8	33.4	35.9	47.3	34.4	24.61	25.2	-2.36		11.179
Sm	2.74	8.44	8.90	11.06	8.57	6.38	6.2	2.96		3.725
Eu	0.91	2.74	2.74	3.44	2.84	2.04	2.06	-1.03		1.335
Gd	2.57	7.82	7.84	9.79	7.99	6.19	6.4	-3.32		5.077
Tb	0.39	1.18	1.07	1.44	1.16	0.99	0.96	2.81		0.885
Dy	2.01	6.03	5.45	6.99	5.88	5.37	5.2	3.29		6.304
Ho	0.35	1.04	0.92	1.25	1.03	1.00	0.99	1.33		1.342
Er	0.88	2.64	2.26	3.09	2.58	2.72	2.4	13.14		4.143
Tm	0.11	0.31	0.27	0.38	0.30	0.34	0.33	2.61		0.621
Yb	0.62	1.82	1.47	2.18	1.78	2.10	2.02	3.75		3.900
Lu	0.09	0.24	0.19	0.28	0.23	0.29	0.29	-1.36		0.589
U/Pb	0.47	0.50	0.98	0.65	0.67					0.15
Th/U	2.16	2.21	1.98	2.13	1.82					2.63
Nb/U	32.0	32.9	31.0	30.4	21.5					49.3
Ce/Pb	29.6	30.3	66.3	39.0	35.2					24.5
La/Nb	0.84	0.79	0.91	0.88	1.08					1.11
Nb/Ta	14.8	14.9	16.9	17.0	16.9					18.3
$(La/Sm)_N$	1.72	1.70	1.84	2.15	1.95					0.67
$(Nd/Sm)_N$	1.29	1.30	1.32	1.32	1.40					0.98
$(Tb/Yb)_N$	2.86	2.95	3.31	3.00	2.96					1.03
$(Ce/Yb)_N$	7.7	7.9	11.5	10.5	9.1					0.85

Trace elements were analyzed by ICP-MS except Cr and Ni, which were analyzed by XRF. Concentrations (ppm) were normalized on a waterfree basis simultaneously with the major element analyses.

*Standard sample (Govindaraju, 1994); **Difference in percentage between working value of Govindaraju (1994) and measured mean of two analyses; ***Values from Hofmann (1988); ****n.d. = not determined; $(. . .)_N$ = normalized to C1 chondrite of Sun and McDonough (1989).

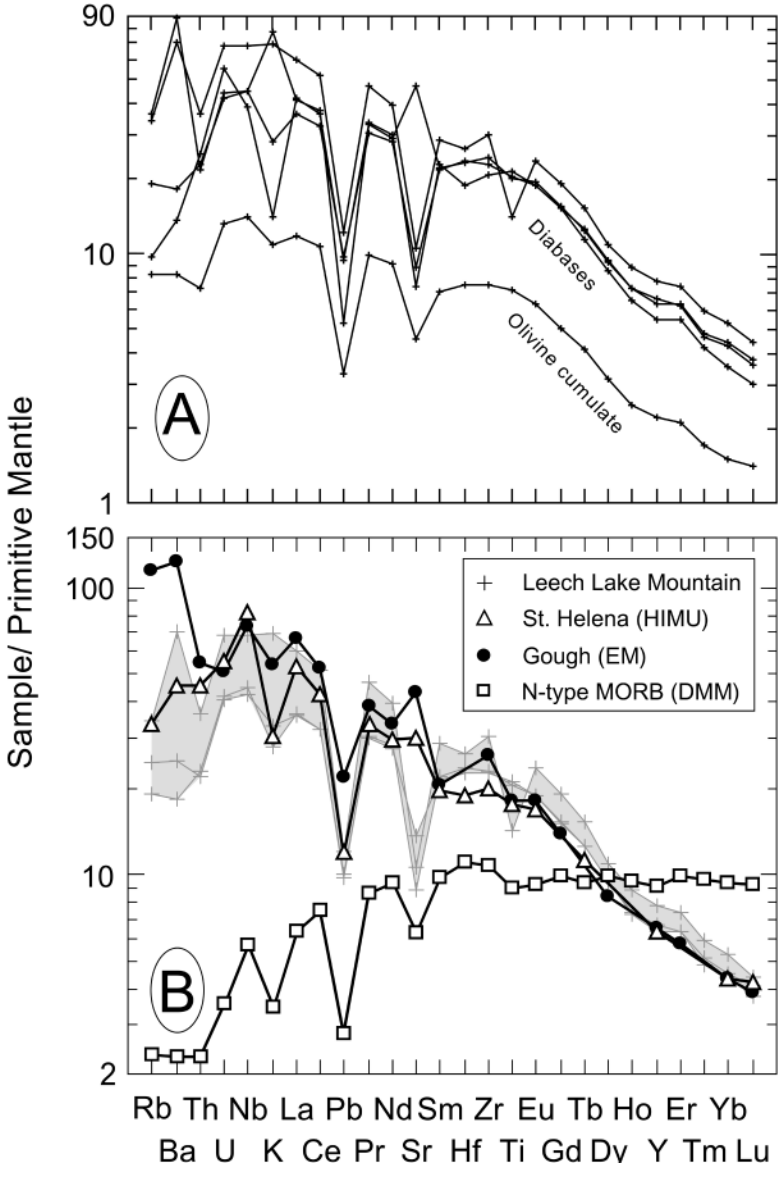

Fig. 6. Primitive mantle (Sun and McDonough 1989) normalized trace element patterns of the Leech Lake Mountain intrusive rocks. (A) Diabases and olivine cumulate. (B) Leech Lake Mountain diabases (grayed field) compared to selected oceanic island basalts and MORB (Mid-Ocean Ridge Basalt). St.Helena data (HIMU (High $^{238}U/^{204}Pb$) source) from Chaffey, Cliff, and Wilson (1989), Gough data (EM (Enriched Mantle) source) from Sun and McDonough (1989), and N-type MORB (DMM (Depleted MORB Mantle) source) data from Hofmann (1988).

considered to be relatively immobile. Sr displays a distinct negative anomaly for most samples but is high in severely altered samples. These samples have a high CaO content and contain considerable amounts of carbonate with a Sr content of up to 3 wt percent. Since plagioclase, the major Sr bearing phase, is not a significant fractionating phase it is suggested that both high and low Sr contents are caused by plagioclase alteration.

The marked inflection at Ti in the pattern of the most fractionated hawaiitic sample Pb-g is caused by magnetite fractionation. The olivine cumulate (sample P1) displays the smoothest trace element pattern and probably represents the most pristine values despite the fact that the olivine is partly serpentinized. If it is corrected for fractionation by subtraction of olivine a good match with sample db II (table 3) is achieved.

Compared to N-type MORB (fig. 6B), the diabases incompatible elements ranging from Rb to Dy are variably enriched whereas the less incompatible elements Ho to Lu are depleted. Incompatible element enrichement is also visible in a chondrite-normalized Rare Earth Element (REE) diagram (not shown). La has values 94 to 156 times chondritic, and Lu ranges from 9 to 11 times chondritic. The Light Rare Earth Elements (LREE) are fractionated from the Heavy Rare Earth Elements (HREE) as expressed by a $(Ce/Yb)_N$ ratio of 8 to 11. Fractionation of the HREE is shown by a $(Tb/Yb)_N$ ratio of 3. In figure 6B only least altered diabases (Pb-g, dbII, $P1_{corrected}$) are plotted. Comparison to ocean island basalts (OIB) from Gough and St. Helena with MgO contents comparable to sample dbII reveals similarities, in particular with St. Helena. Although the Gough pattern fits well with the Leech Lake Mountain diabase pattern from Sm to Lu, the highly incompatible elements are enriched more strongly.

$^{40}Ar/^{39}Ar$ Data

The results of the step heating $^{40}Ar/^{39}Ar$ measurements on kaersutitic amphibole, and phlogopite are presented in table 4. The corresponding apparent age spectra are shown in figure 7. The amphibole yields a plateau for the middle and high temperature degassing steps of 119.0 ± 0.4 Ma, comprizing ~70 percent of the ^{39}Ar released. This age is interpreted as age of diabase intrusion. Low temperature discordance of the amphibole data is associated with anomalously low Ca/K of < 2, suggesting the presence of a K-rich phyllosilicate, which may be manifesting ^{39}Ar recoil phenomena.

The phlogopite yields a more discordant age spectrum than the amphibole and no well defined plateau. The hump-shaped low and middle temperature portion of the age spectrum, which is also reflected by the K/Ca ratios (fig. 7) may be a consequence of ^{39}Ar recoil redistribution involving intracrystalline secondary chlorite, observed in thin section. In such cases, the integrated age of micas has turned out to be geologically significant (Hess and Lippolt, 1986). However, the low apparent step ages of the phlogopite during low temperature degassing could also be caused by radiogenic Ar loss. Therefore, we regard the phlogopite integrated age of 114.9 ± 0.5 Ma as minimum intrusion age. We do not consider the hiatus between amphibole and phlogopite ages as a result of slow cooling of the diabase. Using the mathematical procedure described by Turcotte and Schubert (1982) to model conductive cooling of a sill, it can be estimated that solidification of the 70 m thick sill P1 takes approx 70 yrs. Cooling of the sill border facies from 500°C (approx amphibole Ar closure temperature) to 300°C (approx phlogopite Ar closure temperature) may be in the same order of magnitude, and thus would not cause significant age differences in the two minerals.

CONSTRAINTS FROM ANALYTICAL DATA

Crystal Fractionation

Field observations, petrography, and major element variation indicate that particularly the thicker diabase sills are internally differentiated. Olivine is the first phase on the liquidus, because it occurs as phenocrysts in the chilled margins and in the cumulate. Augite follows olivine on the liquidus, as indicated for example by the continously decreasing CaO and CaO/Al_2O_3 (not shown) in the variation diagrams (fig. 5). The inflection point at 5 percent MgO marks when titano-magnetite joins the liquidus, because TiO_2 and FeO rapidly decrease at lower MgO contents. This is best demonstrated in the plot TiO_2 versus Zr (fig. 5), because both elements are immobile in response to alteration.

TABLE 4

Step heating Ar isotope data on amphibole and phlogopite (J = 0.008605)

Sample step	Mol ^{40}Ar	$^{37}Ar_{Ca}/^{39}Ar_K$	±1σ	$^{40}Ar_{rad}/^{39}Ar_K$	±1σ	$\%^{40}Ar_{rad}$	Apparent age [Ma]	±1σ
Laboratory No. 8257-01 (Kaersutitic amphibole)								
A	3.43E-15	0.506	0.277	4.494	2.726	11.5	68.45	40.74
B	1.79E-14	1.159	0.029	0.952	0.275	5.6	14.71	4.24
C	3.59E-14	1.642	0.019	2.294	0.180	14.1	35.26	2.75
D	1.80E-13	1.699	0.011	4.047	0.102	26.1	61.76	1.53
E	2.44E-13	0.583	0.004	8.169	0.020	92.6	122.56	0.29
F	2.16E-13	0.516	0.003	7.985	0.019	97.1	119.88	0.27
G	1.38E-13	0.871	0.005	7.948	0.022	96.8	119.35	0.31
H	1.33E-13	1.662	0.007	7.924	0.022	96.7	119.00	0.30
I	1.75E-13	2.094	0.012	7.901	0.030	97.1	118.67	0.42
J	4.40E-13	4.717	0.038	7.952	0.031	97.1	119.41	0.40
K	2.31E-13	4.818	0.025	7.916	0.026	97.7	118.88	0.32
L	2.48E-13	5.228	0.026	7.911	0.028	97.9	118.81	0.34
M	3.85E-13	6.486	0.052	7.923	0.029	96.9	118.99	0.31
N	8.25E-14	15.418	0.069	8.138	0.057	84.5	122.10	0.47
O	3.08E-14	12.390	0.060	8.065	0.073	76.7	121.05	0.90
P	8.88E-15	9.806	0.122	8.477	0.513	49.0	127.02	7.41
Q	6.95E-15	7.937	0.168	7.069	0.966	30.4	106.53	14.14
R	4.38E-15	14.757	0.272	0.886	1.167	40.1	13.70	17.97
						Integrated age:	116.3	0.6
Laboratory No. 8258-01 (Phlogopite)								
A	9.05E-14	0.359	0.006	1.413	0.081	12.3	21.81	1.25
B	7.76E-14	0.929	0.009	4.243	0.083	33.7	64.69	1.24
C	1.30E-13	0.174	0.002	3.891	0.033	52.0	59.41	0.50
D	2.56E-13	0.032	0.001	7.562	0.021	83.3	113.74	0.30
E	4.74E-13	0.016	0.001	8.083	0.026	93.1	121.31	0.38
F	4.29E-13	0.015	0.001	8.135	0.027	96.3	122.06	0.40
G	4.69E-13	0.013	0.001	8.026	0.028	97.0	120.48	0.41
H	3.84E-13	0.024	0.001	7.971	0.028	96.4	119.68	0.41
I	3.53E-13	0.044	0.001	7.863	0.024	96.0	118.11	0.35
J	4.06E-13	0.044	0.001	7.764	0.040	96.5	116.67	0.58
K	5.14E-13	0.034	0.001	7.816	0.046	96.9	117.43	0.68
L	6.98E-13	0.035	0.001	7.783	0.024	97.4	116.95	0.35
M	3.43E-13	0.100	0.001	7.825	0.035	97.4	117.55	0.50
N	1.09E-13	0.534	0.005	7.798	0.025	98.0	117.17	0.37
O	4.96E-14	1.301	0.011	7.803	0.051	94.8	117.25	0.73
P	5.00E-14	0.856	0.008	7.908	0.038	97.5	118.77	0.55
Q	7.16E-15	0.476	0.050	7.846	0.360	79.0	117.86	5.24
R	8.92E-15	1.035	0.084	8.006	0.751	29.1	120.19	10.91
S	9.00E-15	1.011	0.121	8.777	1.096	22.4	131.36	15.82
						Integrated age:	114.9	0.5

Major element least square mass balance calculations, based on Bryan, Finger, and Chayes (1969) and using Igpet version 2.0 petrologic software, support the above observations that all samples are related to the most primitive sample db II by fractional crystallization of olivine, augite, and magnetite. The degree of fractionation is moderate, ranging from 10 to 40 percent. The olivine cumulate P1 requires 64 percent olivine addition, that is, P1 = 36 percent db II + 64 percent olivine, and the augite cumulate K I essentially 31 percent augite addition. Residuals are high compared to what is acceptable on the basis of analytical errors. This is most probably caused by gain and loss of silica and alkalies by alteration. In addition, fractionation was modeled using the thermodynamic modeling program MELTS (Ghiorso, Hirsch-

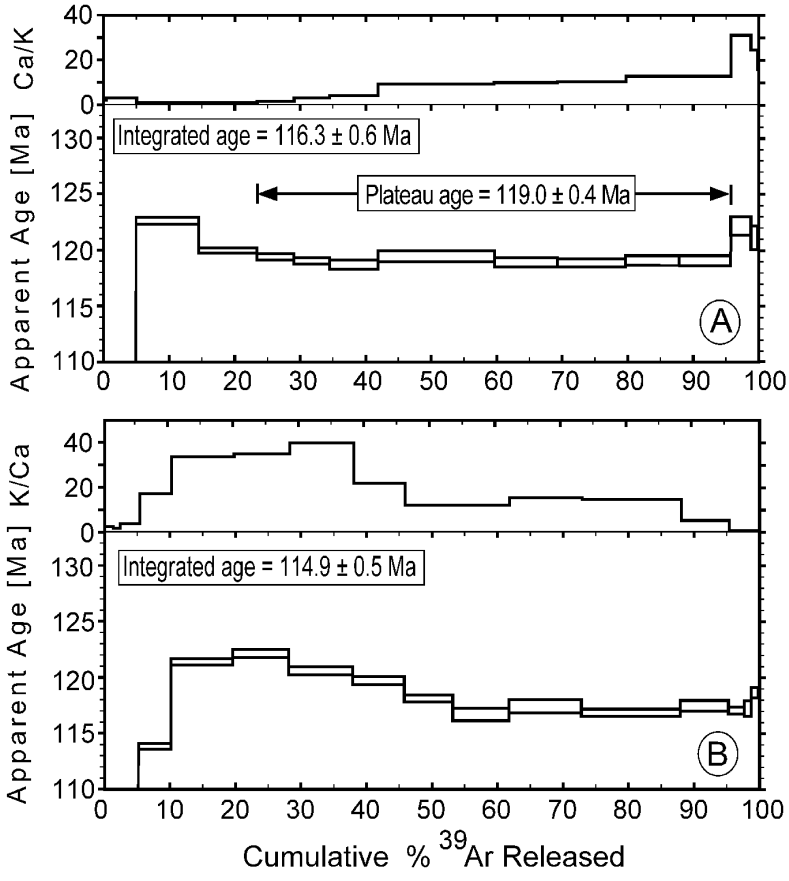

Fig. 7. $^{40}Ar/^{39}Ar$ step heating spectra for kaersutitic amphibole (A) and phlogopite (B).

mann, and Sack, 1994). The results are similar to the least square mass balance calculations and are plotted as liquid lines of descent in figure 5.

In order to estimate a primary magma composition for the Leech Lake Mountain diabases olivine was added to the most primitive sample db II until its composition met the requirements for equilibrium with mantle olivine and to account for the effects of prior fractional crystallization. Since clinopyroxene commonly begins to crystallize between 7 and 8 wt percent MgO in basaltic melts (Nielsen, 1990), it can be assumed that olivine was the only phase fractionating the primary magma from the most primitive rocks found at Leech Lake Mountain. Adding 10 percent of olivine (Fo_{84}) to sample db II results in a magma composition considered to be a minimum estimate for a primary magma: 12 wt percent MgO, Mg# = 66, 496 ppm Cr, 250 ppm Ni, and an equilibrium olivine composition of $Fo_{86\text{-}88}$ (table 5). Equilibrium olivine is calculated assuming $K_{D ol\text{-}liq}^{Mg\text{-}Fe} = 0.27–0.33$. An equilibrium olivine of $Fo_{86\text{-}88}$ is low compared to that of most lherzolites (Fo_{90}; Arai 1987) but is typical for melts in equilibrium with mantle pyroxenite (Hirose and Kushiro 1993). Such a source rock can produce Na_2O and FeO rich, silica undersaturated melts (Hirschmann, Baker, and Stolper, 1995; Cousens, 1996) at high pressures similar to those of Leech Lake Mountain.

Major element composition and fractionating mineral assemblage of the Leech Lake Mountain intrusives are similar to alkali basaltic and basanitic volcanic rocks of

TABLE 5

Calculated primary melt composition (oxides in wt%, elements in ppm). See text for discussion.

Sample	db II	db II +10% olivine
SiO_2	46.42	45.73
TiO_2	3.71	3.35
Al_2O_3	12.53	11.28
Fe_2O_3	2.14	2.18
FeO	10.70	10.91
MnO	0.24	0.24
MgO	8.34	12.02
CaO	10.29	9.29
Na_2O	2.81	2.53
K_2O	0.87	0.78
P_2O_5	0.59	0.53
Total	98.63	98.84
Mg#	58	66
P	2578	2316
Ti	22271	20110
Ni	103	250
Cr	284	496
K	7220	6473
Sr	160	146
Y	25	23
Zr	222	203
Nb	28	25
Ta	1.87	1.71
Hf	6.30	5.75
Sc	21.70	20.54
Pb	1.71	1.56
Th	1.87	1.71
U	0.85	0.78
La	22.24	20.35
Ce	51.73	47.27
Pr	7.39	6.75
Nd	33.42	30.54
Sm	8.44	7.72
Eu	2.74	2.51
Gd	7.82	7.15
Tb	1.18	1.08
Dy	6.03	5.51
Ho	1.04	0.96
Er	2.64	2.42
Tm	0.31	0.28
Yb	1.82	1.66
Lu	0.24	0.22

many oceanic islands and seamounts, for example Tahiti, Tristan da Cuna, Gough, Guadelupe Island, Vesteris seamount, St. Helena, Juan Fernandez Islands (Batiza, 1977; Le Roex, 1985; Baker and others, 1987; Chaffey, Cliff, and Wilson, 1989; Le Roex, Cliff, and Adair, 1990; Duncan and others, 1994; Haase and Devey, 1994). Most of these islands follow a silica-undersaturated differentiation trend with the ultimate differentiation products being nepheline-bearing phonolites.

Partial Melting

Major element constraints.—The effect of pressure and degree of partial melting on basalt composition are graphically represented in the olivine-diopside-plagioclase-quartz tetrahedron (fig. 8) after Kushiro (1996). The normative projection is from

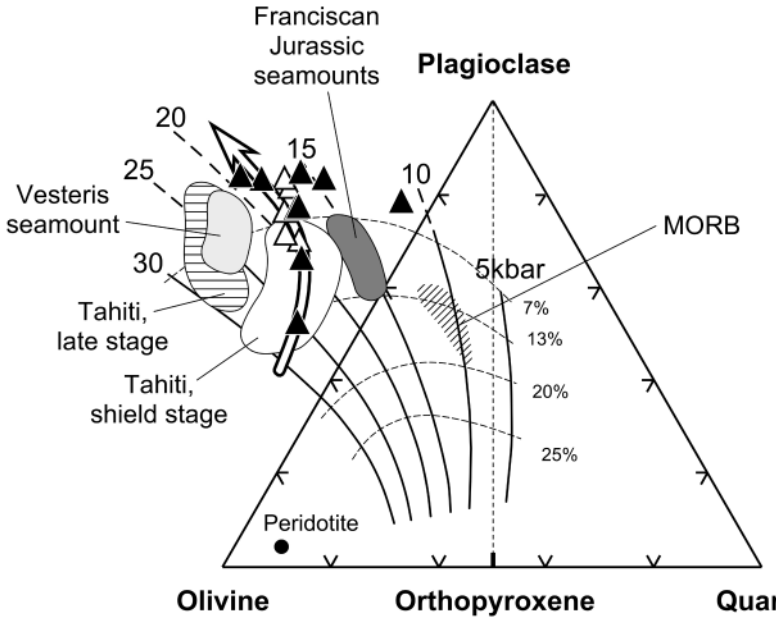

Fig. 8. Isobaric melt composition trends occurring with increasing degree of melting. Triangles: Leech Lake Mountain intrusive rocks; filled: this work; open: Layman (1977). Dashed lines represent degree of melting, heavy arrow is fractionation trend of Tahitian shield stage alkali basalts (Duncan and others, 1994), hatched field is main cluster of MORB given by Walker, Shibata, and DeLong (1979). References for other data fields are given in figure 5. Samples from literature have MgO >7wt percent.

diopside onto the olivine-quartz-plagioclase face using the algorithm of Walker, Shibata, and Delong (1979). At high pressures and small degrees of melting (F) partial melts are silica-undersaturated, rich in FeO but low in Al_2O_3 and CaO. Lower pressures and higher degrees of melting produce silica-saturated partial melts with lower FeO and higher CaO. At pressures $>$ 15 kb and F $<$ 10 percent compositions are alkali basaltic. Olivine tholeiites are produced at 10 to 20 kb and F = 10 to 20 percent. The Leech Lake Mountain diabases appear to have been formed at high pressures (up to about 27 kb) and moderate degrees of melting (F$<$ 15 percent). Most of the diabases define a narrow trend away from the SiO_2 apex, closely matching the fractionation trend of shield stage alkali basalts from Tahiti. The three Leech Lake Mountain diabases that do not follow this trend shift toward the SiO_2 apex and are the most altered samples, indicating the sensitivity of Walker, Shibata, and DeLong's (1979) projection to small losses in alkalies and silica caused by alteration.

Trace element modeling.—Trace element modeling can be used to constrain degree and depth of partial melting as well as source characteristics (Chauvel and Jahn, 1984; McKenzie and O'Nions, 1995; Haase, 1996). In this work, fractional melting is used in our Rare Earth Element modeling. The corresponding equation relating the trace element concentration in the unmelted solid C_0 to that of the extracted melt C_L in the case of nonmodal melting is given by Shaw (1970). Mineral-melt distribution coefficients applied are given in app. B. Aim of the modeling is to most closely fit the entire spectrum of REE to the observed pattern of the primitive Leech Lake Mountain intrusive rocks (db II, Pb-g, P1). Samples Pb-g (40 percent fractionation compared to db II) and P1 (64 percent olivine accumulation) are corrected for crystal fractionation to the composition of db II using the partition coefficents in app. B.

The modeling variables are source composition, source mineralogy, and degree of melting. Source compositions (app. C) start with either fertile garnet lherzolite (PHN 1611, Smith, Griffin, and Ryan, 1992), primitive mantle (Hofmann, 1988), or MORB source (McKenzie and O'Nions, 1995), and may have been modified by addition of melt (fig. 9F). Source mineralogy is chosen analogous to a fertile spinel lherzolite Z-37 from Zabargad Island (Bonatti, 1986). To produce the corresponding garnet lherzolite mineral mode, the reaction olivine + garnet ($grossular_{0.25}$ $pyrope_{0.75}$) = 2.5 enstatite + spinel + 0.75 diopside from Johnson (1990) was applied. Melting modes (app. D) are taken from Johnson (1990). All mantle phases are assumed to remain residual in the partial melted lherzolite, because none of them is melted out at degrees of melting ranging from 0.1 to 10 percent.

First, REE patterns are calculated from a MORB source either with spinel or garnet bearing lherzolite mineralogies. The spinel lherzolite pattern (fig. 9A) is

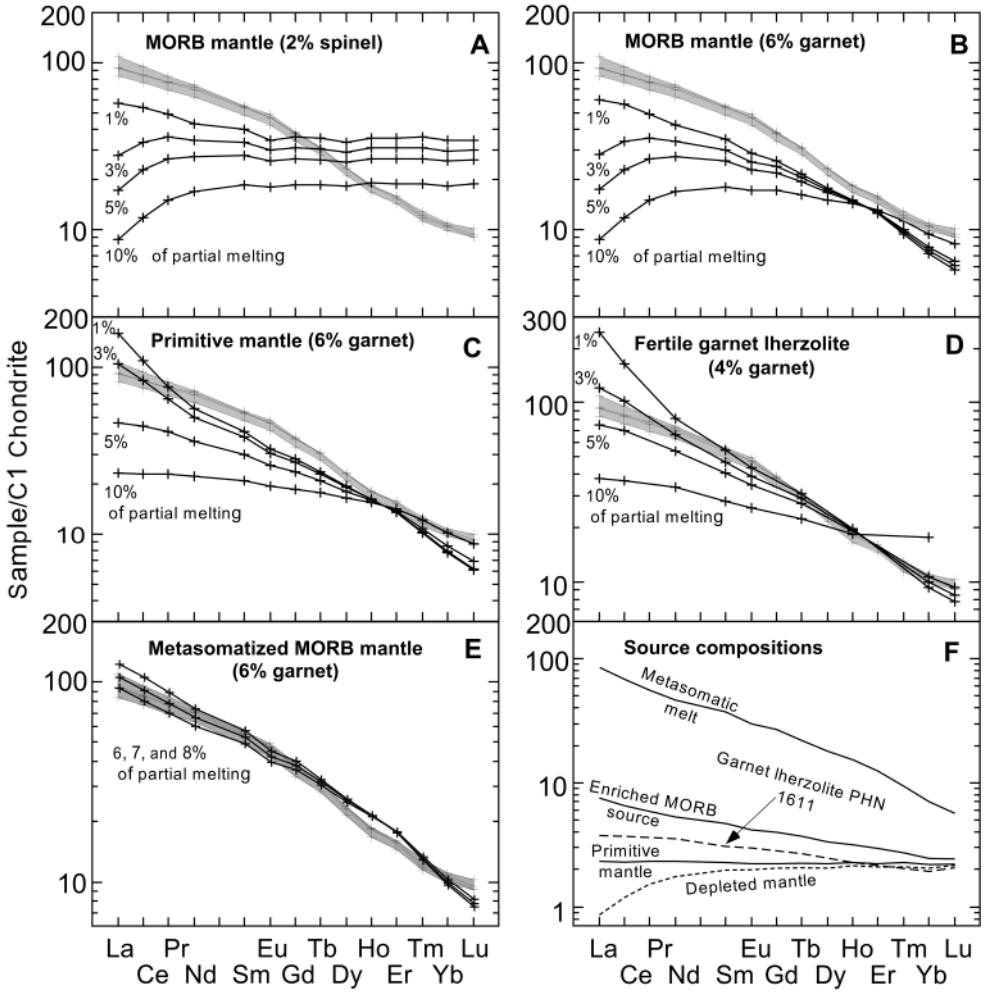

Fig. 9. Melting models used to approach the Leech Lake Mountain diabase REE pattern (grayed field). Type of melting process is aggregate fractional melting. Normalizing values are from Sun and McDonough (1989). See text for discussion.

unfractionated in the HREE and not considered further. The garnet lherzolite pattern (fig. 9B) shows HREE fractionation but is too depleted to match the Leech Lake Mountain pattern even at a low degree of melting of 1 percent. Partial melting of primitive mantle (fig. 9C) yielded higher abundances in LREE, but the elements from Sm to Dy remained too low and La, Ce are slightly too high. Considering the uncertainties in the distribution coefficients and mineral proportions, partial melting of primitive mantle at less than 3 percent with 4-5 percent garnet in the source reasonably well replicates the observed REE pattern of the Leech Lake Mountain intrusive rocks. The best fit, however, was achieved by 6 to 8 percent of partial melting of a MORB source enriched by 8 percent of a metasomatic melt (fig. 9E). 6 percent of garnet in the source are required to account for the fractionated HREE pattern. With this starting composition a good fit is also achieved for most immobile trace elements ranging from Th to Sc. The metasomatic melt was formed by about 0.3 percent melting of MORB mantle in the garnet stability field and is highly enriched in incompatible elements. Such a metasomatically enriched MORB source was used by McKenzie and O'Nions (1995) to account for the observed composition of seamount magmas that cannot be modeled by partial melting of either the MORB or the primitive source. A good fit with the Leech Lake Mountain diabase trace element pattern was achieved by melting the natural garnet lherzolite PHN 1611 (fig. 9D; 3 percent of partial melting in the presence of 4 percent garnet). This garnet lherzolite is a naturally occurring example for an apparently primitive peridotite that was produced by enrichment of a once depleted residue by a metasomatic melt fraction (Smith, Griffin, and Ryan, 1992) and supports the model of a metasomatically enriched MORB source.

Modeling results from alkaline intraplate seamount rocks in the northern Pacific imply the presence of amphibole in the source (Cousens, 1996). Amphibole is a candidate to hold the LILE (Large Ion Lithophile Elements, for example, Cs, Rb, K, Ba) and LREE, and its presence possibly accounts for higher H_2O and CaO/Al_2O_3 observed in the seamount lavas. In this work, small amounts of amphibole <3 percent in the modeled source are permissible without significantly altering the REE pattern. However, considering the more immobile elements from Th to Sc (not shown), distinct anomalies are produced at Y, Ti, Hf, and a general enrichment of the elements that are more incompatible than Pb. Our modeling results do not require the presence of amphibole in the source as a holder of the enriched components.

Summarized, small degrees of partial melting of an enriched garnet-bearing source can account for the trace element patterns of the Leech Lake Mountain rocks. The presence of garnet indicates a depth of melting of 60 to 80 km representing the position of the garnet-spinel transition zone depending on mantle temperature. The garnet-bearing source must be enriched in incompatible elements compared to the MORB source and can either be primitive mantle or MORB source mantle, which was metasomatically enriched by a small melt fraction.

Age of Intrusion

The $^{40}Ar/^{39}Ar$ amphibole age of 119.0 ± 0.4 Ma is the first magmatic age reported for the northern Franciscan Complex and represents the age of diabase sill intrusion into a chert-graywacke sedimentary pile. Other data for coherent blueschists are considered to represent metamorphic ages and are based essentially on K-Ar whole rock and $^{40}Ar/^{39}Ar$ whole rock total fusion dating of metagraywackes and metabasalts (Suppe and Armstrong, 1972; Lanphere, Blake, and Irwin, 1978; Suppe and Foland, 1978; McDowell and others, 1984; Jayko and Blake, 1989). Ages range from 116 to 90 Ma for the Yolla Bolly terrane, whereas the age scatter is possibly caused by disturbances of the isotopic K-Ar system. Assuming the oldest whole-rock age from the Yolla Bolly terrane of 116 Ma as geologically meaningful, that is, the time of peak metamorphism or subsequent cooling through the blocking temperature of Ar, the diabase

intrusion is only about 3 my older. This is consistent with subduction and metamorphism shortly after magmatic activity. The northern California Yolla Bolly terrane is often correlated with the Eylar Mountain terrane of the central California Diablo Range, based on similar lithologies and metamorphic grade (Murchey and Blake, 1993; Blake and others, 1988). However, a magmatic age of 95.0 ± 0.5 Ma and a metamorphic age of 92.1 ± 1.4 Ma was obtained for the Diablo Range Ortigalita Peak gabbro by U/Pb dating of zircon and sphene and an albite + pumpellyite + quartz paragenesis, respectively (Mattinson and Echeverria, 1980). This confirms the concept of Echeverria (1980) that the Ortigalita Peak gabbro intruded at the site of plate convergence, closely followed by subduction and metamorphism about 3 my later. Compared to our Leech Lake Mountain age results this implies that parts of the northern California Yolla Bolly terrane may have been subducted almost 25 my earlier than rocks of the Eylar Mountain terrane. Rapid subduction within a time interval of at least 3 my is generally compatible with plate motion reconstructions (Engebretson, Cox, and Gordon, 1985), showing a marked increase in convergence velocity from 1cm/yr to 7cm/yr at about 135 Ma. Ring and Brandon (1999) estimated a structural burial of 1 km for each 4 km of subduction. Hence, subduction to a depth of 28 km (about 8 kb, as indicated by jadeitic clinopyroxene) would occur within 1.6 my.

Source

Ratios of highly incompatible elements can be used to monitor source composition, because the extent of fractionation from each other by partial melting and differentiation processes is relatively small. Some of the highly incompatible elements in particular the LILE are rather mobile during alteration and low grade metamorphism. This restricts the use of these elements in order to characterize the source in our case. However, three samples, the most primitive rock (db II), the most fractionated rock (Pb-g), and the olivine cumulate (P1) are least affected by alteration and display the smoothest trace element patterns. Plotting incompatible element ratios (table 6) versus La (immobile) as a differentiation index (not shown), it is possible to distinguish between the effects of crystal fractionation and alteration. Alteration causes offset from the trend defined by samples P1, db II, and Pb-g. In table 6 only the values of sample P1 are listed, because they are least affected by alteration.

On the basis of distinct isotope characteristics different mantle components can be distinguished that contribute in varying proportions to the usually mixed sources of oceanic basalts: DMM (Depleted MORB Mantle), HIMU (high μ ($=^{238}U/^{204}Pb$)), and EM (Enriched Mantle). The suggested components FOZO (Hart and others, 1992) and C (Hanan and Graham, 1996) are not considered, because they can not be well characterized on the basis of incompatible element ratios.

The HIMU component is characterized by low $^{87}Sr/^{86}Sr$ and high $^{206}Pb/^{204}Pb$ ratios. The corresponding time-integrated parent-daughter element ratio Rb/Sr is low ($<$ about 0.03) and U/Pb is high ($>$ about 0.3). The primitive mantle normalized element pattern from Nb to Rb displays a continous decrease (fig. 6B; for example, St. Helena OIB), similar to N-type MORB. This relative depletion particularly in Rb and Ba distinguishes the HIMU from the EM component and is consistent with low time-integrated Rb/Sr ratios inferred from low $^{87}Sr/^{86}Sr$ ratios, indicating a depleted heritage of both the HIMU and the MORB source (Hofmann, 1997). Models for HIMU-type mantle generation include recycling of altered oceanic crust (Hofmann, 1997) or migration of CO_2-rich silicate melts from the depleted mantle into the lithosphere (Sun and McDonough, 1989). The enriched mantle source EM has high $^{87}Sr/^{86}Sr$ ratios and is considered to be a product of mantle enrichment by water rich fluids in a subduction zone or by sediment subduction. The high Pb concentration, inherited from the sediments, is reflected by low Ce/Pb and low U/Pb compared to the HIMU source (Sun and McDonough, 1989).

TABLE 6

Leech Lake Mountain intrusive rocks incompatible element ratios compared to ratios from selected mantle reservoirs

	PRIMA	EM	HIMU	LLM	N-type MORB
U/Pb	0.12		0.48	0.47	0.15
Th/U	4.0	4.6	3.6	2.2	2.6
Nb/U	30	43	48	32	49
Nb/Th	7.6	9.3	13.3	14.8	18.7
Ce/Pb	9	20	33	30	25
La/Nb	1.0	0.9	0.7	0.8	1.1
Zr/Nb	16	6	4	8	30
Ba/Nb	10	15	5	6	4
Rb/Nb	0.9	0.9	0.3	0.5	0.4
Rb/Ba	0.09	0.06	0.08	0.09	0.09
Nb/Ta	18		18	15	18
Zr/Hf	36		40	36	35

PRIMA (primitive mantle) and N-type MORB are from Hofmann (1988), EM (Gough Island) and HIMU (St. Helena island) are compiled from Sun and McDonough (1989), Le Roex (1985), and Chaffey, Cliff, and Wilson (1989); LLM (Leech Lake Mountain, sample P1) is from this work.

The Leech Lake Mountain intrusive rocks have high U/Pb, Ce/Pb, Nb/Th, and low La/Nb ratios as well as a relative depletion of U through Rb in the primitive mantle normalized diagram (fig. 6B). The observed characteristics are most compatible with a HIMU-type mantle source. However, Nb/U is unusually low compared to the range of MORB and OIB sources (47 ± 10; Hofmann, 1997). This can be explained as a result of mixture between a HIMU-type source and continental crust sediments. However, since none of the other element ratios, for example, low Ce/Pb indicate sediment addition, the low Nb/U rather reflects alteration. Low Nb/U in conjunction with very low Th/U and high U/Pb can also indicate mobility of U and would weaken the constraints on a HIMU source. However, even the ratios of the mobile elements Rb and Ba point to a HIMU source, and the uniform chondritic ratios of Rb/Ba, Nb/Ta, and Zr/Hf indicate that they have not been significantly modified by alteration.

GEOLOGICAL DISCUSSION

The Oceanic Upper Mantle

Field relationships and age data indicate that the Leech Lake Mountain diabases were emplaced in a chert-graywacke sedimentary pile in a near-trench environment. Consequently, they must have been generated within or beneath the oceanic lithosphere. We suggest that processes and mantle conditions similar to those responsible for the generation of alkaline seamounts can explain the chemistry of the Leech Lake Mountain intrusives, that is, tapping of a metasomatically enriched, HIMU-type melting domain.

Analyses on northeastern and eastern Pacific seamount samples (Batiza and Vanko, 1984; Allan and others, 1989; Niu and Batiza, 1995) show that the underlying mantle is extremly heterogeneous on a small scale. The seamount volcanic rocks range in composition from tholeiitic to alkaline, even within a single volcano, and have a wider range in isotopic compositions than MORB. Seamounts near the northern East Pacific Rise show isotopic mixing arrays between the depleted MORB mantle and the HIMU mantle components (Wendt and others, 1997). Compared to MORB, alkaline

intraplate seamounts have higher H_2O, FeO, LILE, and LREE and lower SiO_2, Mg#, and CaO/Al_2O_3, respectively, consistent with an enriched, amphibole-bearing, probably pyroxenitic source. Seamounts probably tap the same heterogenous mantle source as MORB, but the generally smaller degrees of melting and lack of homogenization lead to greater chemical diversity, which is averaged out by the large melting region and magma pooling beneath spreading centers (Cousens, 1996).

Mantle rocks in ophiolites and xenoliths frequently show that a depleted residue was subsequently enriched by migrating fluids or melts (McDonough and Frey, 1990), confirming metasomatic enrichment of depleted mantle. Highly variable isotopic identity of massive peridotites and pyroxenite veins led Allegre and Turcotte (1986) to propose a model of a two component marble cake mantle consisting of depleted mantle lherzolite and pyroxenitic streaks. While Allegre and Turcotte (1986) suggest the pyroxenitic streaks to be recycled oceanic crust it appears from field observations that they rather represent melts intruded into mantle peridotite. A similar model is used by McKenzie and O'Nions (1995) to account for the observed composition of seamount magmas: metasomatized subcontinental lithosphere near the mechanical boundary layer delaminates caused by a slightly higher density than the sourrounding depleted mantle. It sinks into the convecting upper mantle from where it rises again in hot plumes. The enriched material in the rising plume melts at lower temperatures than the surrounding MORB mantle and produces higher amounts of magma. After some convective overturns the enriched mantle component is dispersed throughout the asthenosphere forming elongated streaks that may still be thick enough to produce lines of seamounts.

Both models support our results from trace element modeling that the Leech Lake Mountain diabases were generated from a metasomatically enriched MORB source.

Age of Lithosphere

In contrast to most northeastern Pacific alkaline seamounts produced in the spinel lherzolite stability field, the Leech Lake Mountain intrusives require a garnet bearing source, indicating a greater depth of melting of at least 60 to 80 km. Using SiO_2 contents of primitive lavas as a barometer Haase (1996) calculated the average depth of melting for intraplate volcanoes and observed a regular increase of depth of melting with increasing age of the lithosphere on which the lavas erupted. He concluded that the average pressures of melting of most magmas lie beneath the thermal boundary layer defined by the 1300°C isotherm. Haase (1996) further reports that the REE ratios, for example, La/Yb, which are essentially invariant at moderate extents of fractional crystallization do systematically increase with sinking SiO_2 of the melts and increasing age of the lithosphere. This indicates the increasing contribution of residual garnet in the source as the depth of melting rises through the spinel-garnet transition zone at approx 80 km depth. These relations imply that the Leech Lake Mountain diabases intruded relatively old lithosphere and explain the lack of garnet in the source of most northeastern Pacific seamount volcanic rocks: They erupted on lithosphere younger than 20 my, indicating a maximum lithospheric thickness of 50 km, which is well above the garnet-spinel transition zone.

Mesozoic Tectonic Setting

How does the occurrence of alkaline magmas, generated beneath aged oceanic lithoshere in a near-trench environment, fit to the Late Mesozoic geotectonic setting of the Californian continental margin and the adjacent oceanic crust?

Blake and others (1988) inferred that the Yolla Bolly terrane, which hosts the Leech Lake Mountain intrusives, represents a collapsed continental margin basin formed in a transtensional or highly oblique convergent setting. Based on radiolarian

chert dating and radiometric ages, Murchey and Blake (1993) studied oceanic residence and arrival times for twelve Franciscan terranes and reconstructed the following plate tectonic history for the Californian continental margin that is in accordance with plate motion reconstructions (Engebretson, Cox, and Gordon, 1985). During Early and early Middle Jurassic the age of the subducted oceanic crust was continously younging until the Klamath-Farallon spreading center approached the trench and was subducted resulting in widespread ophiolite formation at 155 to 164 Ma (Hopson, Mattinson, and Pessagno, 1981; Harper, Saleeby, and Heizler, 1994). Alternative to a single subduction zone, Irwin (1981) has proposed multiple east-dipping subduction zones for the Klamath Mountains during this time frame. In contrast, Cannat and Boudier (1985) have suggested that both east and west dipping subduction occurred. Thereafter, increasing convergence rates were accompanied by large scale Sierra Nevada magmatism and reached a maximum at about 100 Ma, which is coincident with subduction of the oldest oceanic crust. Convergence shifted from left to right lateral movement at this time, and convergence rates almost doubled. During Laramide times subduction got shallower and magmatism migrated into the interior of the continent. This caused cessation of magmatism along the continental margin in the Late Cretaceous.

For the Yolla Bolly terrane this plate tectonic history implies a complex setting governed by changing plate motion from oblique convergent to transcurrent and later convergent again. It can be concluded that the oceanic crust underlying the Yolla Bolly terrane was about 60 my old at the time when small-scale alkalic magmatism occurred. This results from a spreading ridge age of approx 180 Ma (Blake and Murchey, 1993) and the $^{40}Ar/^{39}Ar$ age of 119 Ma for the time of the Leech Lake diabase intrusions. Applying the model of Haase (1996), the thermal boundary layer at an age of 60 Ma should be at a depth of roughly 90 km. This depth is already below the garnet-spinel transition zone. Consequently, the eruption of alkaline magmas with a fractionated HREE pattern like that at Leech Lake Mountain and other locations in the Yolla Bolly terrane is consistent with the assumed thermal properties of the oceanic plate beneath which they were generated.

This is also true for other volcanic rocks in the Franciscan Complex. The Stonyford Volcanic complex (SFVC; Shervais and Hanan, 1989) and the adjacent Snow Mountain complex (SMC; McPherson, 1983) are emplaced in a serpentinite matrix melange between the Coast Range ophiolite and rocks of the northern California Central Belt. They are interpreted as Jurassic on-land seamounts, that is, they were scraped off the oceanic plate and accreted to the Franciscan subduction complex. Both SFVC and SMC consist of thick sequences of pillow lavas, pillow breccias, and subordinate diabase sills and flows as well as interlayered cherts in the upper regions indicating a volcanic hiatus (Shervais and Kimbrough, 1987). On the basis of their transitional to mildly alkaline major element chemistry both seamounts are transitional between young pacific seamounts and the Leech Lake Mountain intrusive rocks. The Stonyford volcanic complex is composed of highly fractionated Ti-rich ferrobasalts and of mildly alkaline hyaloclastite beds with preserved glass, which yield an $^{40}Ar/^{39}Ar$ age of 164 ± 1 Ma (Hanan, Kimbrough, and Renne, 1992). The major element composition of the most primitive glasses from SFVC implies a depth of melting within the spinel lherzolite field. The Ti-rich ferrobasalts in the lower part of the SFVC resemble those associated with propagating rift systems (Shervais and Kimbrough, 1987) or with ridge-transform intersections. If the 10 m thick chert within the SFVC reports a volcanic hiatus of about 10 my, based on a typical accumulation rate of 1mm/kyr (Isozaki and Blake, 1994), the ferrobasalts might have originated at a propagating rift/ridge-transform intersection at 175 Ma, that is, on very young crust. The alkalic capping 10 my later is consistent with aged crust and thicker lithosphere.

The SMC is younger than the SFVC judging from fossil ages (Tithonian to Valanginian, about 150-135 Ma). The rocks are Ti-rich transitional basalts and rare silicic derivatives. McPherson (1983) concludes from petrography that the lavas erupted in shallow water and that the top of the seamount might have been subaerially exposed at some time. This led him to interpret it as a near-ridge seamount. This interpretation is also consistent with a seamount erupted on young ocean crust and is also compatible with Blake and Murchey's (1993) plate tectonic scenario, suggesting the subduction of a spreading center at about 155 Ma. However, the SMC seamount is underlain by abyssal plain and pelagic sediments indicating a distal trench setting and thus the oceanic crust must have aged for several million years prior to eruption of the seamount lavas.

Physical Model

A model for volcanism in a near-trench setting should explain why magma is present in this setting and why it was mobilized and reached the earth surface at that time.

From seismic wave attenuation it is known that a low-velocity zone (LVZ) extends from the base of the rigid lithosphere to a depth of about 250 km. The LVZ or asthenosphere is part of the convecting upper mantle, and the strong attenuation of seismic waves is attributed to the presence of a small melt fraction (McKenzie and O'Nions, 1995). Hole and Saunders (1996) infer the presence of small CO_2 rich melt fractions in a depth of 110 to 130 km (garnet stability field) beneath normal spreading axes, based on trace element inversion on slab window-related basalts. They suggest that such trace element enriched melts contribute to the formation of N-type MORB, but that the trace element signature of these enriched melts is lost during successive melt pooling over a large melting column. Such "MORB precursor melts" can be preserved if the melting column is truncated by a lithospheric cap of up to 50 km thickness as is the case for the slab window-related basalts of Hole and Saunders (1996). Other workers (Chauvel and Jahn, 1984; Le Roex, 1985; Allegre and Turcotte, 1986; McKenzie and O'Nions, 1995) imply the migration of CO_2 rich melts into the suboceanic or continental lithosphere to account for the trace element enrichment of isotopically depleted alkaline rocks. Following the above hypotheses in favor of small fluid-rich melt fractions at the upper mantle-lithosphere boundary, it is possible that they were also present beneath the oceanic lithosphere of the Yolla Bolly terrane.

Many seamounts are related to fractures in the oceanic crust allowing upward migration of magma such as propagating rifts, ridge-transform intersections, fracture zones, failed rifts, and abandoned spreading centers (Batiza and Vanko, 1984; Allan and others 1989; Haase and Devey, 1994). Davis and others (1995) observed a temporal relationship between seamount magmatism offshore southern and Baja California and magmatism in the adjacent continental borderland in response to tectonic plate reorganization events. A similar scenario is suggested for the small scale magmatic activity in the Yolla Bolly terrane documented by intrusion of numerous alkaline diabase sills, for example at Leech Lake Mountain. Highly oblique subduction or transcurrent plate motions are likely to open sufficient pathways for relatively small melt fractions to intrude the sedimentary pile overlying the ocean crust of the Yolla Bolly terrane. Deep sea drilling has shown the presence of off-ridge basaltic sills intercalated in sedimentary sequences at different locations in the ocean basins including continental margin sedimentary prisms (Echeverria, 1980). Compositionally they are both, tholeiitic to mildly alkaline. Echeverria (1980) discusses several settings that can account for magmatism in an accretionary prism: subduction of a spreading ridge, a fracture zone (for example, the Mendocino fracture zone), or the upward bending of the downgoing slab in the subduction zone. Subduction of a spreading ridge segment could be a suitable model. For example, Cole and Basu (1995) attribute a large portion of the Miocene bimodal volcanism in coastal southern California to

ridge-trench interactions during subduction of segments of the Farallon-Pacific spreading center resulting in the formation of the San Andreas fault system. Trace element and isotope data indicate that depleted suboceanic asthenosphere welled up into the opening slab window after ridge-trench collision and replaced the subcontinental lithospheric mantle. However, spreading ridge subduction is not compatible with the relatively old oceanic crust at the Early Cretaceous active continental margin as inferred from Murchey and Blake (1993). Thermal considerations reinforce this argument. Ridge subduction results in elevated geothermal gradients. If this had occurred at the time of intrusion of the Leech Lake diabases, amphibolite facies would be expected at that depth (Wakabayashi, 1996).

Subduction of a fracture zone is more likely as a model for the generation of the Leech Lake Mountain diabases, because it does not require the proximity of a spreading center. A recent example would be the migration of the Mendocino triple junction northward along the California plate margin. Asthenospheric upwelling associated with the passage of the triple junction is considered to have caused the age progressive Late Cenozoic volcanism in the California Coast Ranges (Cole and Basu, 1995). Since seamount volcanism is also frequently associated with fracture zones, this is a very likely mechanism to produce alkaline basalts. However, in contrast to the migrating Mendocino triple junction and associated volcanism, the setting of the Leech Lake intrusive rocks would be subduction of a fracture zone without stoppage of subduction. If subduction had ceased and thermal gradients had risen as documented in the Late Cenozoic Coast Ranges (Cole and Basu, 1995), then the facies of metamorphism would be different as noted above (Wakabayashi, 1996).

CONCLUSIONS

Scattered intrusion of Franciscan sediments by basaltic magma represents small scale magmatic activity in a trench sedimentary environment or in the accretionary prism itself prior to subduction and blueschist facies metamorphism.

The Leech Lake Mountain alkaline diabases are Ti-rich and fractionated olivine, augite, and titaniferous magnetite. Back addition of 10 percent of olivine to the most primitive observed melt can account for fractionation and provides an estimate of a primary magma in equilibrium with a pyroxenitic mantle source. Despite alteration the major element compositions with low SiO_2 and high TiO_2 and FeO are consistent with low degrees of partial melting at high pressures.

Enriched trace element characteristics of the diabases are typical for oceanic island basalts and can be modeled by 6 to 8 percent of partial melting of a MORB source, which was enriched by up to 8 percent of a metasomatic melt. Following a modeling approach of McKenzie and O'Nions (1995), the metasomatic melt is derived by 0.3 percent of partial melting of a garnet-bearing MORB source. About 6 percent of garnet in the mantle source of the diabases can account for the observed heavy REE fractionation and suggest a depth of melting below the garnet-spinel transition zone at 60 to 80 km. This is in agreement with the reconstructed age and thickness of the Early Cretaceous oceanic plate the diabases intruded.

Incompatible trace element ratios of the diabases are consistent with a HIMU-type mantle source. Geochemical studies of Pacific seamounts have shown that the oceanic upper mantle is extremely heterogenous on a small scale and that HIMU-type mantle domains can be tapped by seamount magmatism even in the vicinity of a spreading center. Large degrees of melting and magma pooling beneath a spreading axis effectively average out these enriched signatures. This demonstrates that OIB-like isotopic and trace element signatures are not restricted to mantle plumes rising from great depth.

The Early Cretaceous tectonic setting along the California continental margin is dominated by rapid, highly oblique subduction. If melt is present beneath the oceanic

lithosphere without a thermal anomaly, it may readily percolate upward through conduits opened by transtensional tectonics. Asthenospheric upwelling beneath a fracture zone, which is migrating along the continental margin may be a viable alternative.

$^{40}Ar/^{39}Ar$ dating of kaersutitic amphibole from the diabase yields the first igneous age of 119.0 ± 0.4 Ma for the northern California Franciscan Complex. This age implies rapid subduction and metamorphism a few million years after intrusion of the diabases, corresponding to results from the southern California Ortigalita Peak intrusion.

ACKNOWLEDGMENTS

We wish to thank Karsten Haase for help with ICP-MS analyses as well as John Donovan and Burkhard Schulz-Dobrick for assistance with microprobe analyses. This paper benefitted from discussions with Karsten Haase, Thomas Wenzel and Iris van der Zander. Thorough and helpful reviews by John W. Shervais and John Wakabayashi are highly appreciated. Field work was supported by a scholarship of the University of Mainz to A.J.W. The Covelo Ranger Station provided logistic support during field mapping.

APPENDIX A
Sample Description

P1: Medium-grained olvine cumulate; base of sill; contains augite oikocrysts (2-5 mm); apatite, phlogopite, kaersutitic hornblende and opaques are found in interstices; olivine partly serpentinized.

K I: Medium-grained diabase; rich in euhedral prisms of augite, displaying sector zoning; very likely of cumulate origin; groundmass is chlorite, albite, white mica; large pseudomorphs (up to 5 mm) of chlorite after a long prismatic, skeletal hollow mineral, probably olivine.

Pb-f: Medium-grained diabase with intergranular to subophitic texture; augites are hollow cored slender prisms up to 5 mm; plagioclase forms euhedral to subhedral prisms of about 1 mm.

Pb-g: Medium to coarse-grained leucocratic granular diabase; augite forms euhedral prisms up to 7 mm; plagioclase is mostly euhedral up to 4 mm in length.

PLII: Medium-grained diabase with granular to subophitic texture; lower central part of a sill; augite forms prisms of up to 2 mm; plagioclase occurs as up to 4 mm long laths, frequently subhedral; chlorite pseudomorphs after probably olivine.

PL2: Medium-grained diabase with intersertal texture; base of sill; augite is skeletal hollow and almost completely replaced by chlorite, sphene, pumpellyite, and glaucophane.

db I: Coarse-grained diabase with ophitic texture; subhedral augites (2-3 mm) partly enclose cruciform skeletal titanomagnetite and euhedral plagioclase laths (typically about 1.5 mm).

db II: Fine to medium-grained diabase with granular texture; base of sill; augite occurs as euhedral prisms and is zoned; plagioclases are euhedral to subhedral; abundant polyhedral or more irregular chlorite pseudomorphs after probably olivine.

db-u: Medium-grained intersertal or intergranular diabase from upper third of sill; plagioclase forms elongated laths of up to 8 mm; mafic minerals almost completely replaced by chlorite and carbonate.

Appendix B

Partition coefficients used for trace element modeling

	Partition coefficient K_D					
	Olivine	Orthopyroxene	Clinopyroxene	Spinel	Amphibole	Garnet
Cr	0.3	1.5	3.0	300	0.34	5.5
Ni	9.4	9.4	9.4			
Co	1.0	2.0	2.0	2.0	1.4	2.0
K	0.0002	0.001	0.002	0.0001	1.2	0.001
Sr	0.0002	0.007	0.13		0.12	0.0011
Y	0.005	0.028***	0.295***		1	2.11
Sc	0.16	0.33	1.7**		0.75*	2.27
Ti	0.02	0.1	0.18	0.15	1.5	0.28
Zr	0.01	0.03	0.1		0.5	0.32
Hf		0.01	0.22		0.14*	0.25***
Nb	0.005	0.005	0.02		0.8	0.07
Ta	0.005	0.005	0.02		0.38	0.04
Th	0.0001	0.0001	0.00026		0.011*	0.0001
U	0.0001	0.0001	0.00036		0.01*	0.0001
Pb	0.0001	0.0013	0.01		0.1	0.0005
La	0.0004	0.002	0.054	0.01	0.17	0.01
Ce	0.0005	0.003	0.098	0.01	0.26	0.021
Pr	0.0008	0.0048	0.15	0.01	0.35	0.054
Nd	0.001	0.0068	0.21	0.01	0.44	0.087
Sm	0.0013	0.01	0.26	0.01	0.76	0.217
Eu	0.0016	0.013	0.31	0.01	0.88	0.32
Gd	0.0015	0.016	0.3	0.01	0.86	0.498
Tb	0.0015	0.019	0.31	0.01	0.83	0.75
Dy	0.0017	0.022	0.33	0.01	0.78	1.06
Ho	0.0016	0.026	0.31	0.01	0.73	1.53
Er	0.0015	0.03	0.3	0.01	0.68	2.0
Tm	0.0015	0.04	0.29	0.01	0.64	3.0
Yb	0.0015	0.049	0.28	0.01	0.59	4.03
Lu	0.0015	0.06	0.28	0.01	0.51	5.5

Data from McKenzie and O'Nions (1991, 1995) except for those marked.
*Zack, Foley, and Jenner (1996); **Arth (1976); ***interpolated values.

Appendix C

Source compositions used for modeling

	Metasomatic melt	E-type MORB	PHN 1611	MORB source	Primitive mantle
Cr	2600.94	2968.08		3000.00	3000.00
Ni	226.49	1858.12	1935.00	2000.00	2000.00
Co	78.44	102.88		105.00	105.00
K	6617.93	547.83	1442.00	20.00	200.00
Sr	705.46	69.96	38.40	14.70	20.00
Y	18.19	4.38		3.18	3.45
Sc	22.87	12.87		12.00	12.00
Ti	14492.06	2097.76	1500.00	1020.00	1020.00
Zr	159.02	19.34		7.19	8.51
Hf	4.55	0.57		0.22	0.25
Nb	31.19	2.85		0.39	0.54
Ta	1.68	0.15		0.02	0.03
Th	2.33	0.19		0.01	0.07
U	0.60	0.05		0.00	0.02
Pb	4.45	0.37		0.02	0.16
La	20.10	1.80	0.89	0.21	0.55
Ce	41.97	4.02	2.25	0.72	1.40
Pr	5.33	0.56		0.14	0.22
Nd	21.70	2.49	1.65	0.82	1.08
Sm	5.66	0.73	0.47	0.30	0.35
Eu	1.73	0.24	0.17	0.12	0.13
Gd	5.51	0.83		0.42	0.46
Tb	0.83	0.14	0.10	0.08	0.08
Dy	4.58	0.85		0.53	0.57
Ho	0.86	0.18	0.13	0.12	0.13
Er	2.08	0.49		0.35	0.37
Tm	0.24	0.07		0.05	0.06
Yb	1.21	0.42	0.33	0.35	0.37
Lu	0.14	0.06	0.05	0.05	0.06

Unit is ppm. MORB source and primitive mantle data from McKenzie and O'Nions (1995); PHN 1611 = fertile garnet lherzolite (Smith, Griffin, and Ryan, 1992); E-type MORB = MORB source enriched by 8 percent metasomatic melt; metasomatic melt = partial melt from 0.3 percent of fractional melting of MORB source.

Appendix D

Mineral modes of mantle sources used for modeling

	Spinel lherzolite		Garnet lherzolite	
	source (wt%)	melting mode (wt%)	source (wt%)	melting mode (wt%)
Olivine	63	10	66	5
Orthopyroxene	19	20	14	5
Clinopyroxene	16	68	14-16	40
Spinel	2	2		
Hornblende				
Garnet			6-4	50

References

Allan, J.F., Batiza, R., Perfit, M.R., Fornari, D.J., and Sack, R.O., 1989, Petrology of lavas from the Lamont seamount chain and adjacent East Pacific Rise, 10° N: Journal of Petrology, v. 30, p. 1245–1298.

Allegre, C.J., and Turcotte, D.L., 1986, Implications for a two-component marble-cake mantle: Nature, v. 323, p. 123–127.

Arai, S., 1987, An estimation of the least depleted spinel peridotite on the basis of olivine-spinel mantle array: Neues Jahrbuch für Mineralogie, Monatshefte, v. 8, p. 347–354.

Arth, J.G., 1976, Behavior of trace elements during magmatic processes - a summary of theoretical models and their applications: Journal of Research of the United States Geological Survey, v. 4, p. 41–47.

Baker, P.E., Gledhill, A., Harvey, P.K., and Hawkesworth, C.J., 1987, Geochemical evolution of the Juan Fernandez Islands, SE Pacific: Journal of the Geological Society London, v. 144, p. 933–944.

Batiza, R., 1977, Petrology and chemistry of Guadalupe Island: an alkalic seamount on a fossil ridge crest: Geology, v. 5, p. 760–764.

Batiza, R. and Vanko, D., 1984, Petrology of young Pacific seamounts: Journal of Geophysical Research, v. 89, no. B13, p. 11,235–11,260.

Blake, M.C., Jayko, A.S., McLaughlin, R.J., and Underwood, M.B., 1988, Metamorphic and tectonic evolution of the Franciscan Complex, Northern California, *in* Ernst, W.G., editor, Metamorphism and crustal evolution of the Western United States: Rubey-Volume no. 7, p. 1035–1060.

Bonatti, E., Ottonello G., and Hamlyn, P.R., 1986, Peridotites from the island of Zabargad, Red sea: petrology and geochemistry: Journal of Geophysical Research, v. 91, no. B1, p. 599–631.

Bryan, W.B., Finger, L.W., and Chayes, F., 1969, Estimating proportions in petrographic mixing equations by least-squares approximation: Science, v. 163, p. 926–927.

Burchfiel, B.C., Cowan, D.S., and Davis, G.A., 1992, Tectonic overview of the Cordilleran orogen in the Western United States, *in* Burchfiel, B.C., Lipman, P.W., and Zoback, M.L., editors, The Cordilleran orogen, Conterminous U.S.: Geological Society of America, Geology of North America, v. G-3, p. 407–480.

Cannat, M., and Boudier, F., 1985, Structural study of intra-oceanic thrusting in the Klamath Mountains, northern California: Implications on accretion geometry: Tectonics, v. 4, p. 435–452.

Chaffey, D.J., Cliff, R.A., and Wilson, B.M., 1989, Characterization of the St. Helena magma source, *in* Saunders, A.D. and Norry, M.J., editors, Magmatism in the ocean basins: Geological Society Special Publication 42, p. 257–276.

Chauvel, C., and Jahn, B.M., 1984, Nd-Sr isotope and REE geochemistry of alkali basalts from the Massif Central, France: Geochimica et Cosmochimica Acta, v. 48, p. 93–110.

Chesterman, C.W., 1963, Intrusive ultrabasic rocks and their metamorphic relationships at Leech Lake Mountain, Mendocino County, California, *in* Short Contributions to California Geology: California Division of Mines and Geology, Special Report 82, p. 1–10.

Cloos, M., 1986, Blueschists in the Franciscan Complex of California petrotectonic constraints on uplift mechanisms, *in* Evans, B.W., and Brown, E.H., editors, Blueschists and eclogites: Geological Society of America Memoir 164, p. 77–93.

Cole, R.B. and Basu, A.R., 1995, Nd-Sr isotopic geochemistry and tectonics of ridge subduction and Middle Cenozoic volcanism in Western California: Geological Society of America Bulletin, v. 107, no. 2, p. 167–179.

Cousens, B.L., 1996, Depleted and enriched upper mantle sources for basaltic rocks from diverse tectonic environments in the Northeast Pacific ocean: the generation of oceanic alkaline vs. tholeiitic basalts, *in* Basu, A., and Hart, S., editors, Earth processes: Reading the isotopic code: American Geophysical Union, Geophysical Monograph 95, p. 207–231.

Cox, K.G., Bell, J.D., Pankhurst, R.J., 1979, The interpretation of igneous rocks: London, George Allen and Unwin, p. 1–445.

Davis, A.S., Gunn, S.H., Bohrson, W.A., Gray, L.B., and Hein, J.R., 1995, Chemically diverse, sporadic volcanism at seamounts offshore Southern and Baja California: Geological Society of America Bulletin, v.107, no. 5, p. 554–570.
Donaldson, C.H., 1982, Spinifex-textured komatiites: a review of textures, compositions and layering, *in* Arndt, N.T. and Nisbet, E.G., editors, Komatiites: London, George Allen and Unwin, p. 213–245.
Donovan, J.J., and Tingle, T.N., 1996, An improved mean atomic number background correction for quantitative microanalysis: Journal of Microscopy, v. 2, no. 1, p. 1–7.
Duncan, R.A., Fisk, M.R., White, W.M., and Nielsen, R.L., 1994, Tahiti: Geochemical evolution of a French Polynesian volcano: Journal of Geophysical Research, v. 99, no. B12, p. 24,341–24,357.
Echeverria, L.M., 1980, Oceanic basaltic magmas in accretionary prisms: the Franciscan intrusive gabbros: American Journal of Science, v. 280, p. 697–724.
Engebretson, D.C., Cox, A., and Gordon, R.G., 1985, Relative motion between oceanic and continental plates in the Pacific basin: Geological Society of America Special Paper 206, p. 1–59.
Ernst, W.G., 1979, Coexisting sodic and calcic amphiboles from high-pressure metamorphic belts and the stability of barroisitic amphibole: Mineralogical Magazine, v. 43, p. 269–278.
——— 1988, Tectonic history of subduction zones inferred from retrograde blueschist P-T paths: Geology, v. 16, p. 1081–1084.
Evans, B.W., 1990, Phase relations of epidote-blueschists: Lithos, v. 25, p. 3–23.
Garbe-Schönberg, C.D., 1993, Simultaneous determination of thirty-seven trace elements in twenty-eight international rock standards by ICP-MS: Geostandards Newsletter, v. 17, no. 1, p. 81–97.
Ghiorso, M.S., Hirschmann, M.M., and Sack, R.O., 1994, New software models – thermodynamics of magmatic systems: EOS transactions, v. 75, p. 574–576.
Ghiorso, M.S., and Sack, R.O., 1995, Chemical mass transfer in magmatic processes: a revised and internally consistent thermodynamic model for the interpolation and extrapolation of liquid-solid equilibria in magmatic systems: Contributions to Mineralogy and Petrology, v. 119, no. 2–3, p. 197–212.
Govindaraju, K., 1994, 1994 Compilation of working values and sample description for 383 geostandards: Geostandards Newsletter, v. 18, p. 1–158.
Haase, K.M., 1996, The relationship between the age of the lithosphere and the composition of oceanic magmas: Constraints on partial melting, mantle sources and the thermal structure of the plates: Earth and Planetary Science Letters, v. 144, p. 75–92.
Haase, K.M., and Devey, C.W., 1994, The Petrology and geochemistry of Vesteris seamount, Greenland Basin -an intraplate alkaline volcano of non-plume origin: Journal of Petrology, v. 35, p. 295–328.
Hagstrum, J.T., and Murchey, B.L., 1993, Deposition of Franciscan Complex cherts along the paleoequator and accretion to the American continental margin at tropical paleolatitudes: Geological Society of America Bulletin, v. 105, p. 766–778.
Hanan, B., and Graham, D., 1996, Lead and helium isotope evidence from oceanic basalts for a common deep source of mantle plumes: Science, v. 272, no. 5264, p. 991–995.
Hanan, B.B., Kimbrough, D.L., and Renne, P.R., 1992, The Stonyford volcanic complex: a Jurassic seamount in the Northern California Coast Ranges: American Association of Petroleum Geologists Bulletin, v. 76, no. 3, p. 421–432.
Hanson, G.N., 1990, An approach to trace element modeling using a simple igneous system as an example, *in* Lipin, B.R., and McKay, G.A., editors, Geochemistry and mineralogy of the Rare Earth Elements: Mineralogical Society of America, Reviews in Mineralogy 21, p. 79–97.
Harper, G.D., Saleeby, J.B., and Heizler, M., 1994, Formation and emplacement of the Josephine ophiolite- and the age of the Nevadan orogeny in the Klamath Mountains, California-Oregon: U/Pb zircon and $^{40}Ar/^{39}Ar$ geochronology: Journal of Geophysical Research, v. 99, p. 4293–4321.
Hart, S.R., Hauri, E.H., Oschmann, L.A., and Whitehead, J.A., 1992, Mantle plumes and entrainment: isotopic evidence: Science, v. 256, no. 5056, p. 517–520.
Hess, J.C., and Lippolt, H.J., 1986, Kinetics of Ar isotopes during neutron irradiation: ^{39}Ar loss from minerals as a source of error in $^{40}Ar/^{39}Ar$ dating: Chemical Geology, Isotope Geoscience section, v. 59, p. 223–236.
Hirose, K., and Kushiro, I., 1993, Partial melting of dry peridotites at high pressures: determination of compositions of melts segregated from peridotite using aggregates of diamond: Earth and Planetary Science Letters, v. 114, p. 477–489.
Hirschmann, M.M., Baker, M.B., and Stolper, E.M., 1995, Partial melting of mantle pyroxenite: EOS (American Geophysical Union), v. 76, p. 696.
Hofmann, A.W., 1988, Chemical differentiation of the earth: the relationship between mantle, continental crust, and oceanic crust: Earth and Planetary Science Letters, v. 90, p. 297–314.
——— 1997, Mantle geochemistry: the message from oceanic volcanism: Nature, v. 385, p. 219–229.
Hole, M.J., and Saunders, A.D., 1996, The generation of small melt-fractions in truncated melt columns: constraints from magmas erupted above slab windows and implications from MORB genesis: Mineralogical Magazine, v. 60, p. 173–189.
Hopson, C.A., Mattinson, J.M., and Pessagno, E.A. Jr., 1981, The Coast Range ophiolite, western California, *in* Ernst, W.G., editor, The geotectonic development of California:, Englewood Cliffs, New Jersey, Prentice-Hall, p. 419–510.
Hussong, D.M., and Uyeda, S., 1981, Tectonic processes and the history of the Mariana Arc: a synthesis of the results of Deep Sea Drilling Project Leg 60, Initial reports, Deep Sea Drilling Project, Leg 60: Initial reports of the Deep Sea Drilling Project, v. 60, p. 909–929.
Irwin, W.P., 1981, Tectonic accretion of the Klamath Mountains, *in* Ernst, W.G., editor, The geotectonic development of California: Englewood Cliffs, New Jersey, Prentice-Hall, p. 29–49.
Isozaki, Y., and Blake, M.C., 1994, Biostratigraphic constraints on formation and timing of accretion in a subduction complex: an example from the Franciscan Complex of Northern California: Journal of Geology, v. 102, no. 3, p. 283–296.

Jayko, A.S., and Blake, M.C.,1989, Deformation of the Eastern Franciscan Belt, Northern California: Journal of Structural Geology, v. 11, no. 4, p. 375–390.
Jayko, A.S., Blake, M.C., and Brothers, R.N., 1986, Blueschist metamorphism of the Eastern Franciscan Belt, Northern California, *in* Evans, B.W. and Brown, E.H., editors, Blueschists and eclogites: Geological Society of America Memoir 164, p. 107–123.
Jochum, K.P., and Seufert, H.M., 1990, Multi-element analysis of 15 international standard rocks by isotope-dilution spark source mass spectrometry: Geostandards Newsletter, v. 14, p. 469–473.
Johnson, K.T.M, Dick, H.J.B,, and Shimizu, N., 1990, Melting in the oceanic upper mantle: an ion microprobe study of diopsides in abyssal peridotites: Journal of Geophysical Research, v. 95, no. B3, p. 2661–2678.
Kuno, H., 1966, Differentiation of basalt magmas, *in* Hess, H.H., and Poldervaart, A., editors., Basalts: The Poldervaart treatise on rocks of basaltic composition 2: New York, Interscience, p. 623–688.
Kushiro, I., 1996, Partial melting of a fertile mantle peridotite at high pressures: an experimental study using aggregates of diamond, *in* Basu, A., and Hart, S., editors, Earth processes: Reading the isotopic code: American Geophysical Union, Geophysical Monograph 95, p. 109–122.
Lanphere, M.A., Blake, M.C., and Irwin, W.P., 1978, Early Cretaceous metamorphic age of the South Fork Mountain Schist in the Northern Coast Ranges of California: American Journal of Science, v.278, p. 798–815.
Layman, E.B., 1977, Intrusive rocks in the near-trench environment: two localities in the Northern California Franciscan Complex: M.S. thesis, Palo Alto, California, Stanford University, p. 1–56.
Leake, B.E., 1978, Nomenclature of amphiboles: American Mineralogist, v. 63, p. 1023–1052.
LeRoex, A.P., 1985, Geochemistry, mineralogy and magmatic evolution of the basaltic and trachytic lavas from Gough Island, South Atlantic: Journal of Petrology, v. 26, p. 149–186.
LeRoex, A.P., Cliff, R.A., and Adair, B.J., 1990, Tristan da Cunha, South Atlantic: geochemistry and petrogenesis of a basanite-phonolite lava series: Journal of Petrology, v. 31, p. 779–812.
MacPherson, G.J., 1983, The Snow Mountain volcanic complex: an on-land seamount in the Franciscan terrain, California: Journal of Geology, v. 91, p. 73–92.
Mattinson, J.M., and Echeverria, L.M., 1980, Ortigalita Peak gabbro, Franciscan Complex, U-Pb dates of intrusion and high-pressure-low-temperature metamorphism: Geology, v. 8, p. 589–593.
McDonough, W.F., and Frey, F.A., 1989, Rare earth elements in upper mantle rocks, *in* Lipin, B.R., and McKay, G.A., editors, Geochemistry and mineralogy of the Rare Earth Elements: Mineralogical Society of America, Reviews in Mineralogy 21, p. 100–145.
McDowell, F.W., Lehman, D.H., Gucwa, P.R., Fritz, D., and Maxwell, J.C., 1984, Glaucophane schists and ophiolites of the Northern California Coast Ranges: isotopic ages and their tectonic implications: Geological Society of America Bulletin, v. 95, p. 1373–1382.
McKenzie, D., and O'Nions, R.K., 1995, The source regions of oceanic island basalts: Journal of Petrology, v. 36, p. 133–159.
McKenzie, D., and O'Nions, R.K., 1991, Partial melt distributions from inversion of rare earth element concentrations: Journal of Petrology, v. 32, p. 1021–1091.
Moore, D.E., and Blake, M.C., 1989, New evidence for polyphase metamorphism of glaucophane schist and eclogite exotic blocks in the Franciscan Complex, California and Oregon: Journal of Metamorphic Geology, v. 7, p. 211–228.
Murchey, B.L., and Blake, M.C.,1993, Evidence for subduction of a major ocean plate along the California margin during the Middle to early Late Jurassic, *in* Dunne, G.C. and McDougall, K.A., editors, Mesozoic paleogeography of the Western United States: Society for Sedimentary Geology Field Trip Guidebook, Pacific Section, v. 71, p. 1–18.
Niu, Y., and Batiza, R., 1995, Extreme mantle source heterogeneities beneath the Northern East Pacific Rise: trace element evidence from near-ridge seamounts: EOS (Transactions American Geophysical Union), v. 76, p. 654.
Renne, P.R., 1995, Excess ^{40}Ar in biotite and hornblende from the Norils'k 1 intrusion: Implications for the age of the Siberian Traps: Earth and Planetary Science Letters, v. 131, p. 165–176.
Renner, R., Nisbet, E.G., Cheadle, M.J., Arndt, N.T., Bickle, M.J., and Cameron, W.E., 1994, Komatiite flows from the Reliance Formation, Belingue Belt, Zimbabwe: I. Petrography and Mineralogy: Journal of Petrology, v. 35, p. 361–400.
Renne, P.R., Swisher, C.C., Deino, A.L., Karner, D.B., Owens, T., and DePaolo, D.J., 1998, Intercalibration of Standards, Absolute Ages and Uncertainties in $^{40}Ar/^{39}Ar$ Dating: Chemical Geology (Isotope Geoscience Section), v. 145 (1–2), p. 117–152.
Ring, U., and Brandon, M.T, 1999, Ductile deformation and mass loss in the Franciscan subduction complex: implications for exhumation processes in accretionary wedges, *in* Ring U., Brandon, M.T., Lister, G.S., and Willett, S.D., editors, Exhumation processes: Normal faulting, ductile flow and erosion: Geological Society London, Special publications, v. 154, p. 55–86.
Ringwood, A.F., and Irifune, T., 1988, Nature of the 650-km seismic discontinuity: implications for mantle dynamics and differentiation: Nature, v.331, p. 131–136.
Robinson, P., 1980, The composition space of terrestrial pyroxenes, *in* Previtt, C.T., editor, Reviews in Mineralogy 7, Pyroxenes: Mineralogical Society of America, p. 419–494.
Roeder, P.L., and Emslie, R.F., 1970, Olivine liquid equilibrium: Contributions to Mineralogy and Petrology, v. 29, p. 275–289.
Shaw, D.M., 1970, Trace element behavior during anatexis: Geochimica et Cosmochimica Acta, v. 34, p. 237–243.
Shervais, J.W., and Hanan, B.B., 1989, Jurassic volcanic glass from the Stonyford volcanic complex, Franciscan assemblage, Northern California Coast Ranges: Geology, v. 17, p. 510–514.
Shervais, J.W., and Kimbrough, D.L., 1987, Alkaline and transitional subalkaline metabasalts in the

Franciscan Complex melange, California, *in* Morris, E.M., and Pasteris, J.D., editors, Mantle metasomatism and alkaline magmatism: Geological Society of America Special Paper 215, p. 165–182.
Simonetti, A., Shore, M., and Bell, K., 1996, Diopside phenocrysts from nephelinite lavas, Napak volcano, Eastern Uganda: evidence for magma mixing: Canadian Mineralogist, v.34, p. 411–421.
Smith, D., Griffin, W.L., and Ryan, C.G., 1993, Compositional evolution of high-temperature sheared lherzolite PHN 1611: Geochimica et Cosmochimica Acta, v. 57, p. 605–613.
Steiger, R.H., and Jäger, E., 1977, Subcommission on geochronology: Convention on the use of decay constants in geo- and cosmochronology: Earth and Planetetary Science Letters, v. 36 p. 359–362.
Sun, S.S., and McDonough, W.F., 1989, Chemical and isotopic systematics of oceanic basalts: implications for mantle composition and processes, *in* Saunders, A.D. and Norry, M.J., editors, Magmatism in the ocean basins: Geological Society Special Publication 42, p. 313–345.
Suppe, J., 1973, Geology of the Leech Lake Mountain-Ball Mountain region, California: Berkeley, University of California Press, p. 1–81.
Suppe, J. and Armstrong R.L., 1972, Potassium-argon dating of Franciscan metamorphic rocks: American Journal of Science, v. 272, p. 217–233.
Suppe, J., and Foland, K.A., 1978, The Goat Mountain schists and Pacific Ridge Complex: a redeformed but still-intact Late Mesozoic schuppen complex, *in* Howell, D.G., and McDougall, K.A., editors, Mesozoic paleogeography of the Western United States: Society of Economic Paleontologists and Mineralogists Pacific Section, Pacific Coast Paleogeographic Symposium 2, p. 431–451.
Taylor, R.N., Marlow, M.S., Johnson, L.E., Taylor, B., Bloomer, S.H., and Mitchell, J.G., 1995, Intrusive volcanic rocks in Western Pacific forearcs, *in* Taylor, B., and Natland, J., editors, Active Margins and Marginal Basins of the Western Pacific: American Geophysical Union, Geophysical Monograph 88, p. 31–43.
Terabayashi, M., and Maruyama, S., 1998, Large pressure gap between the Coastal and Central Franciscan belts, northern and central California: Tectonophysics, v. 285, p. 87–101.
Turcotte, D.L., and Schubert, G., 1982, Geodynamics: New York, Wiley and Sons, p. 1–334.
Wakabayashi, J., 1990, Counterclockwise P-T-t paths from amphibolites, Franciscan Complex, California: Metamorphism during the early stages of subduction: Journal of Geology, v. 98, p. 657–680.
——— 1992, Nappes, tectonics of oblique plate convergence, and metamorphic evolution related to 140 million years of continuous subduction, Franciscan Complex, California: Journal of Geology, v. 100, no. 1, p. 19–40.
——— 1996, Tectono-metamorphic impact of a subduction-transform transition and implications for interpretation of orogenic belts: International Geology Review, v. 38, p. 657–680.
Walker, D., Shibata, T., and DeLong, S.E., 1979, Abyssal tholeiites from the Oceanographer Fracture Zone III: phase equilibria and mixing: Contributions to Mineralogy and Petrology, v. 70, p. 111–125.
Wendt, J.I., Niu, Y., Batiza, R., and Regelous, M., 1997, Extreme mantle source heterogeneities beneath the Northern East Pacific Rise: trace element and Nd-Pb-Sr isotope evidence from near-ridge seamounts: European Union of Geosciences, Abstract Supplementary No. 1, Terra Nova, v. 9, p. 60.
Winchester, J.A., and Floyd, P.A., 1977, Geochemical discrimination of different magma series and their differentiation products using immobile elements: Chemical Geology, v. 20, p. 325–343.
Winterer, E.L., Natland, J.H., Van Waasbergen, R.J., Duncan, R.A., McNutt, M.K., Wolfe, C.J., Premoli Silva, I., Sager, W.W., and Sliter, W.V., 1993, Cretaceous guyots in the Northwest Pacific: an overview of their geology and geophysics, *in* Pringle, M.S., Sager, W.W., Sliter, W.V., and Stein, S., editors, The Mesozoic Pacific: geology, tectonics, and volcanism: American Geophysical Union, Geophysical Monograph 77, p. 307–334.
Zack, T., Foley, S.F., and Jenner, G.A., 1996, A consistent trace element partition coefficient set of 21 trace elements for clinopyroxene, amphibole and garnet through laser ablation microprobe analysis of garnet pyroxenites from Kakanui, New Zealand: Goldschmidt Conference, Sixth, Heidelberg, Germany, Journal for Conference Abstracts, 1 (1), p. 691.